Effect of steam voids on in-core detector response in boiling water reactors

by

Harold Herman Paustian

A Thesis Submitted to the
Graduate Faculty in Partial Fulfillment of
The Requirements for the Degree of
MASTER OF SCIENCE

Department: Chemical Engineering and Nuclear Engineering
Major: Nuclear Engineering

Iowa State University
Ames, Iowa

1975

TABLE OF CONTENTS

LIST OF FIGURES

LIST OF TABLES

I. INTRODUCTION

One of the most distinctive features of a boiling water reactor (BWR) is that bulk boiling of the moderator-coolant, usually light water, not only is allowed, but indeed is the major means of heat transfer within the reactor core. This means that in a large portion of a BWR core, the coolant flowing through fuel bundles is a mixture of liquid water and steam bubbles at a pressure of about 1000 psia. In light water reactors, the coolant also acts as a moderator to slow fast neutrons to thermal energies where the probability of a fission event occurring is much greater. Because steam bubbles have a negligible moderating ability, they are often called "steam voids", although the bubbles are not true voids but simply are of such low density as to have little effect. Thus, the presence of steam voids and the volume fraction that such voids occupy has a very significant effect upon neutron parameters such as diffusion length and the ratio of fast flux to thermal flux.

Neutron detectors depend upon some type of reaction with neutrons as a physical basis for their operation. The relative probability of this reaction occurring will depend upon the energy of the neutrons impinging upon the detector. If the detector has a significant cross section for fast neutrons, as do some self-powered neutron detectors, then knowledge of the ratio of fast flux to thermal flux is important in interpreting the signal produced by these detectors. Knowledge of the magnitude of the ratio of fast flux to thermal flux is also important in interpreting the results of neutron noise measurements, since random fluctuations in the void fraction of the coolant will affect the slowing down of fast neutrons and ultimately the signal produced by the detector.

In this study, the main thrust is toward obtaining an idea of what magnitude the ratio of fast flux to thermal flux is and how much it varies as one moves from the bottom of the core to the top of the core in a typical BWR fuel bundle. A sinusoidal axial power shape is assumed, and a void fraction profile, including the effects of subcooled boiling, is calculated. The void fraction profile calculation employs relationships between quality and void fraction and utilizes empirical slip ratio correlations. After the void fraction profile is computed, this information and composition data and dimensions for a unit cell in a BWR lattice are used as input for the computer code LEOPARD, which computes macroscopic cross sections and diffusion coefficients for a fast neutron group and a thermal neutron group. FOG, a one-dimensional neutron diffusion code, then uses this data to compute axial flux profiles for the fast group and the thermal group. Finally, the application of knowledge of the ratio of the fast flux to the thermal flux to interpretation of detector responses is briefly considered.

Throughout this study, physical data corresponding to the dimensions and operating characteristics of the Duane Arnold Energy Center boiling water reactor (DAEC BWR) is used to obtain representative numerical values. Pertinent data concerning this reactor may be found in Appendix A.

II. LITERATURE REVIEW

The subject of axial variation of the ratio of fast flux to thermal flux in a BWR does not appear to be treated extensively in the available literature. Jaschik and Seifritz [1] take ~ 3.4 as being a typical ratio characteristic of a materials-testing type of reactor moderated by light water when they develop a model for calculating the response of prompt-responding self-powered neutron detectors. Hannaman [2], in an appendix to his Ph.D. dissertation involving the development of a BWR noise model for use in anomaly detection, briefly considered how the ratio of fast flux to thermal flux would affect his model. He considered ratios of 1.5, 5.0, and 10.0, with most of his calculations being based on the value of 1.5. He did not consider, however, any axial variation of this value with variation of the void fraction.

The calculation of void fraction profiles appears more frequently in current literature. Probably the best references in this area are a Ph.D. dissertation by Dix [3] in which an extensive discussion of the advantages and shortcomings of current void fraction calculational models is presented, along with Dix's own contributions based on his experimental work, and a report by Lahey [4] in which he summarizes many of the important concepts and models involved in two-phase flow in boiling water nuclear reactors. Both of these works are good summaries of the current state of understanding of two-phase heat transfer.

A fairly substantial quantity of literature is also available concerning the use of in-core neutron detectors in neutron noise measurements in boiling water reactors. Some of the most recent articles in this area dealing specifically with the use of self-powered neutron detectors for noise measurements in a BWR include the paper by Jaschik and Seifritz [1], a paper summarizing noise measurements made at the Lingen Nuclear Power Plant in Germany [5], and a work describing operating experience and developmental work using various emitter materials in self-powered neutron detectors [6]. Hannaman [2] also considers this, but his concern is more toward an overall noise model for the reactor rather than focusing attention solely on detector response to fluctuations both in neutron level and void content in the surrounding moderator. Self-powered neutron detectors are good candidates for use in an on-line anomaly detection system for boiling water reactors because of their ruggedness and small size. Since such detectors respond to both thermal and fast neutrons, some knowledge of the variation of the ratio of the two fluxes in a BWR seems pertinent.

III. VOID FRACTION PROFILE

A. Introduction

One feature of the BWR most distinguishes it from other nuclear reactors. That feature is that boiling of the coolant is allowed, and that this boiling heat transfer is the predominant mode of heat transfer within the reactor core. The resulting generation of steam bubbles within the water circulating through the core affects a wide spectrum of the operating capabilities of the BWR, ranging from the design of an appropriate load-following system to its inherent stability, via the effects of steam voids upon both the thermal and nuclear properties of the steam-water mixture that serves both as moderator and coolant. Thus, knowledge of the relative proportions of liquid and vapor in the mixture and the manner in which these proportions change as the coolant travels up through the core is important.

The analysis of this two-phase flow is a fairly complicated endeavor and generally requires that at some point one must resort to empirical correlations to completely determine the relative proportions of liquid and vapor present. The applicability of such correlations to conditions different from those used in their formulation is another complicating factor, and some caution must be exercised in the use of these correlations. Although two-phase flow analysis is complex and it not yet completely understood, proper and judicious use of existing models combined with reliable correlations leads to results which have been successfully applied in past BWR design work and which are suitable for the purposes of this study.

Relative proportions of liquid and vapor may be expressed by the quality of the mixture, which is a ratio based on mass, or by the void fraction of the mixture, which is a volume ratio. Since heat flow rates, mass flow rates, heats of vaporization, etc. are usually expressed on a mass basis, the calculation of the quality of the mixture is straightforward. To then determine the corresponding void fraction, however, it is necessary to use some sort of correlation or relationship between quality and void fraction. This correlation accounts for "slip" between the liquid and vapor and averaging effects. Before delving into this further, it is necessary to consider some definitions.

B. Void Fraction and Volumetric Flow Fraction

The void fraction, or vapor fraction, of a two-phase mixture under steady-state conditions is a time-averaged value of the fraction of the total volume containing both liquid and vapor which is occupied by vapor alone. If one imagines a unit volume containing both water and steam bubbles and then imagines that all the steam bubbles could be coalesced into one giant steam bubble, then the fraction of the unit volume occupied by that giant steam bubble would be the void fraction at that particular instant of time. Because of fluctuations in heat input, turbulence in the flowing two-phase mixture, etc., the void fraction is a random variable rather than a deterministic quantity. Thus, to obtain the time-averaged value of the void fraction, one might imagine taking a series of "snapshots" of the flowing mixture at various instants of time under "stable" conditions, and then determining the average of the fraction of a unit volume occupied by steam bubbles. Another interpretation is to consider some fixed position in the mixture at N different instants of time and then to define the void fraction as the fraction of those N observations when the point of interest is in vapor. If the generation of steam voids is a stationary random process, then the Ergodic hypothesis proposes that the time-average value and the ensemble-average value of the void fraction will be the same, and the above interpretations should be equally valid.

For the purposes of this section of this study, the time-average value of the void fraction under steady-state conditions will be the subject of interest, and random fluctuations in the instantaneous value of the void fraction will not be considered. In other words, the void fraction will be treated deterministically, even though in actuality it is a quantity with random characteristics.

From the above discussion, it can be seen that:

$$\alpha \equiv \iiint_{V_g} dV \Big/ \iiint_{V} dV = \frac{V_g}{V} = \frac{V_g}{(V_g + V_\ell)} \tag{3.1}$$

where α is the void fraction, V represents volume, the "g" subscript indicates the "gas" phase, and the "ℓ" subscript indicates the liquid phase. If the steam-water mixture is contained in a tube or a channel oriented in the z-direction, then the above is also equivalent to:

$$\alpha = \Delta z \iint_{A_g} dA/\Delta z \iint_{A} dA = \frac{A_g}{A} = \frac{A_g}{(A_g + A_\ell)} \tag{3.2}$$

where A is the cross-sectional area of the tube or channel and Δz is a differential element of length.

It is also possible to define what is known as a volumetric flow fraction:

$$\beta \equiv \frac{Q_g}{Q_g + Q_\ell} = \frac{j_g}{j_g + j_\ell} \tag{3.3}$$

where β is the volumetric flow fraction, Q is a flow rate in units such as ft^3/hr, and j is a "volumetric flux." Note that:

$$j_g \equiv \frac{Q_g}{A_g + A_\ell} \tag{3.4}$$

$$j_\ell \equiv \frac{Q_\ell}{A_g + A_\ell} \tag{3.5}$$

Thus, the volumetric flux of each phase is just the volumetric flow rate of that phase divided by the cross-sectional area of the tube or channel through which the steam-water mixture is flowing.

Finally, so-called "phase velocities" may be defined:

$$u_g \equiv \frac{Q_g}{A_g} \tag{3.6}$$

$$u_\ell \equiv \frac{Q_\ell}{A_\ell} \tag{3.7}$$

Obviously, the phase velocities and volumetric fluxes are related by:

$$u_g = \frac{Q_g}{A_g} = \frac{Q_g}{A_g + A_\ell}\left(\frac{A_g + A_\ell}{A_g}\right) = \frac{j_g}{\alpha} \tag{3.8}$$

$$u_\ell = \frac{Q_\ell}{A_\ell} = \frac{Q_\ell}{A_g + A_\ell}\left(\frac{A_g + A_\ell}{A_\ell}\right) = \frac{j_\ell}{(1 - \alpha)} \tag{3.9}$$

Then, the volumetric flow fraction could be written as:

$$\beta = \frac{j_g}{j_g + j_\ell} = \frac{\alpha u_g}{\alpha u_g + (1 - \alpha)u_\ell} = \frac{\alpha}{\alpha + (1 - \alpha)(\frac{u_\ell}{u_g})} \tag{3.10}$$

The ratio of the phase velocity of the vapor to that of the liquid is called the slip ratio, S, so that:

$$\beta = \frac{\alpha}{\alpha + (\frac{1 - \alpha}{S})} \tag{3.11}$$

Thus, the manner in which the void fraction and the volumetric flow fraction are related will be dependent upon the degree of "slip" between the water and the steam bubbles.

Further comments are in order at this point. The above relationships treat the flow of the liquid phase and of the steam phase as if all of the water was moving at one characteristic velocity, all of the vapor was moving at a second characteristic average velocity, and this slip ratio was a measure of the "slip" between the two phases. This is a "lumped system" approach to a situation which is actually more complex. Existing within the flowing mixture will be velocity profiles for both the liquid and vapor phases dependent upon geometry effects, turbulence effects, etc. To completely specify these profiles would be a complex, generally unnecessary, and often virtually impossible complication. Instead, the lumped system approach is used. The end result, however, is that the slip ratio not only includes the effects of buoyancy forces upon steam bubbles caused by the density difference between the steam and water, but also includes the effect of replacing velocity profiles by average velocities.

Just as the velocities used in the above expressions are cross-sectional average values, so are the void fractions and volumetric flow fractions cross-sectional averages. Thus, instead of β, $\langle\beta\rangle$ should be written, and $\langle\alpha\rangle$ should replace α. Note that "$\langle\ \rangle$" indicates the cross-sectional averaging expressed by:

$$\langle F\rangle \equiv \frac{1}{A_{CS}} \iint_{A_{CS}} F dA \tag{3.12}$$

where F is some quantity and A_{CS} is the cross-sectional area of the flow. Then, for example, the relation between the void fraction and the volumetric flow fraction would be written as:

$$\langle\beta\rangle = \frac{\langle\alpha\rangle}{\langle\alpha\rangle + \left(\frac{1 - \langle\alpha\rangle}{S}\right)} \tag{3.13}$$

C. Quality

Several different methods of defining the quality of a steam-water mixture also exist. Two of particular interest here are the thermodynamic equilibrium quality, x_e, and the flow quality, x. The thermodynamic equilibrium quality is defined by

$$x_e \equiv \frac{h - h_f}{h_{fg}} \tag{3.14}$$

where h is the enthalpy of the two-phase mixture, h_f is the enthalpy of saturated liquid at the pressure of interest, and h_{fg} is the heat of vaporization at that same pressure. Obviously, x_e can be positive or negative, depending upon whether $h > h_f$ or $h < h_f$. x_e is called the thermodynamic equilibrium quality or "mixing cup" quality because it is the quality that would exist if one imagines dipping a bucket into the flowing steam-water mixture, allowing thermodynamic equilibrium to be reached, and then determining the resulting quality.

Consider briefly what is meant by thermodynamic equilibrium. As the enthalpy of water serving as a coolant is increased, one often thinks of the process according to the following sequence:

$$\begin{matrix}\text{Subcooled} \\ \text{liquid}\end{matrix} + \text{no vapor} \rightarrow \begin{matrix}\text{Saturated} \\ \text{liquid}\end{matrix} + \text{no vapor} \rightarrow \begin{matrix}\text{Liquid-vapor} \\ \text{mixture}\end{matrix}$$

$$\rightarrow \begin{matrix}\text{Saturated} \\ \text{vapor}\end{matrix} + \text{no liquid}$$

There are instances, however, when this is not the sequence of events. One of interest to this study is subcooled boiling. In this situation, some boiling occurs before the average enthalpy, or the bulk enthalpy, of the water reaches the saturated liquid value. Thus, part of the energy being added is going toward producing vapor, while the remaining portion increases the enthalpy of the remaining liquid. Now, thermodynamic equilibrium does not exist in this situation, because if one again imagines dipping an imaginary bucket into the flowing coolant, pulling out a sample, and then setting the sample aside and stirring the sample to assume homogeneity, the vapor bubbles would condense, giving the heat of vaporization to increasing the enthalpy of the liquid. The bulk enthalpy of the sample would remain the same, but its composition would be changed in going from thermodynamic nonequilibrium to thermodynamic equilibrium. The existence of steam bubbles under thermodynamic nonequilibrium conditions may be due to the presence of a "boundary layer" of liquid over the heating surface having a temperature higher than the bulk temperature of the coolant and to the steam bubbles being swept "downstream" to a region having $h > h_f$ before the bubbles "have time" to condense.

At any rate, a second way of defining quality is to define the flow quality by:

$$x \equiv \frac{\rho_g u_g A_g}{\rho_g u_g A_g + \rho_\ell u_\ell A_\ell} \tag{3.15}$$

where ρ_g and ρ_ℓ indicate the densities of the vapor and liquid phases of the mixture respectively. This is the true mass flow fraction of vapor present, regardless of whether or not thermodynamic equilibrium exists and always has a value between 0 and 1.

Again, since cross-sectional average values will be used, the two quality definitions should more properly be written as:

$$\langle x_e \rangle = \frac{\langle h \rangle - h_f}{h_{fg}} \tag{3.16}$$

and

$$\langle x \rangle = \frac{\rho_g u_g A_g}{\rho_g u_g A_g + \rho_\ell u_\ell A_\ell} \tag{3.17}$$

Under conditions of bulk boiling, thermodynamic equilibrium will exist and the above two definitions will become equivalent. When bulk boiling exists, both the liquid and vapor phases will be saturated and adding heat to the steam-water mixture will <u>not</u> increase the enthalpy in Btu/lb_m of <u>either</u> the steam portion or the liquid portion of the mixture, but instead will change the <u>relative proportions</u> of steam and water by converting water into bubbles of vapor.

Recall that for subcooled boiling, the enthalpies in Btu/lb_m of the two phases were not the same. Letting the enthalpies of the liquid and vapor be h_ℓ and h_g respectively, a heat balance (neglecting kinetic and potential energy terms) implies that:

$$\langle h_\ell\rangle(1 - \langle x\rangle) + h_g\langle x\rangle = h_{in} + \frac{1}{GA_{CS}}\int_0^z q'dz \qquad (3.18)$$

where h_{in} is the enthalpy of the coolant entering the core, G is the mass flux or the mass flow rate divided by the cross-sectional area, and q' is the linear heat generation rate. But also note:

$$\langle h\rangle = h_{in} + \frac{1}{GA_{CS}}\int_0^z q'dz \qquad (3.19)$$

where $\langle h\rangle$ is the bulk enthalpy of the two phase mixture. Thus, all that has been said is that the liquid enthalpy plus the vapor enthalpy equals the bulk enthalpy of the mixture. So:

$$\langle h_\ell\rangle(1 - \langle x\rangle) + h_g\langle x\rangle = \langle h\rangle \qquad (3.20)$$

Nearly all the enthalpies and qualities will be functions of the axial position, z, so that a more correct expression is:

$$\langle h_\ell(z)\rangle(1 - \langle x(z)\rangle) + h_g\langle x(z)\rangle = \langle h(z)\rangle \qquad (3.21)$$

or

$$\langle x(z)\rangle = \frac{\langle h(z)\rangle - \langle h_\ell(z)\rangle}{h_g - \langle h_\ell(z)\rangle} \qquad (3.22)$$

Note that h_g has not been written either as $h_g(z)$ or $\langle h_g\rangle$, since in subcooled boiling, one would not expect the vapor phase to have any enthalpy other than its <u>saturation</u> value for that pressure, h_g, which is a constant for a given pressure. Then, looking at the above expression one sees that as $\langle h_\ell(z)\rangle$ approaches the saturated liquid value of h_f, $\langle x(z)\rangle$ becomes equivalent to $x_e(z)$ as thermodynamic equilibrium is reached and bulk boiling begins. It is particularly worthwhile to note that bulk boiling begins when $\langle h_\ell(z)\rangle$ reaches h_f, not when $\langle h(z)\rangle$ reaches h_f.

D. Fundamental Void-Quality Relation

Finally, a relationship between void fraction and quality is reached. One can be easily derived by considering the two identities:

$$G(1 - \langle x\rangle)A_{CS} = \rho_\ell Q_\ell = \rho_\ell(1 - \langle\beta\rangle)Q = \rho_\ell\left[1 - \frac{\langle\alpha\rangle}{\langle\alpha\rangle + (\frac{1 - \langle\alpha\rangle}{S})}\right]Q \tag{3.23}$$

and

$$G\langle x\rangle A_{CS} = \rho_g Q_g = \rho_g\langle\beta\rangle Q = \rho_g\left[\frac{\langle\alpha\rangle}{\langle\alpha\rangle + (\frac{1 - \langle\alpha\rangle}{S})}\right]Q \tag{3.24}$$

Dividing the second equation by the first gives:

$$\frac{\langle x\rangle}{(1 - \langle x\rangle)} = \left(\frac{\rho_g}{\rho_\ell}\right)(S)\left[\frac{\langle\alpha\rangle}{(1 - \langle\alpha\rangle)}\right] \tag{3.25}$$

or

$$\langle\alpha\rangle = \frac{\langle x\rangle}{\left[\langle x\rangle + (S)\left(\frac{\rho_g}{\rho_\ell}\right)(1 - \langle x\rangle)\right]} \tag{3.26}$$

This is a fundamental relationship holding for all conditions. Empirical conditions will become important in determining appropriate values to use for S and the actual physical conditions, geometry, etc. will make themselves felt through their effect on this parameter.

E. Flow Regimes

As the relative proportions of liquid and vapor change in two-phase flow, the bubble-liquid mixture tends to assume various non-homogeneous spatial distributions. Such configurations are often called flow regimes, with the boundaries between various regimes somewhat arbitrarily defined, and may be dependent on such factors as mass flux, heat flux, and geometry effects. Figure 3.1 indicates some of the typical flow regimes that can exist for vertical flow and Figure 3.2 indicates how the transitions from regime to regime can progress with increasing heat flux and/or changing axial position.

In general, these flow regimes do not enter explicitly into void and quality relationships for several reasons:

1) The boundary between two regimes is arbitrarily defined.

2) The likelihood of a particular flow regime existing may depend on a large number of parameters, some of which may be difficult to quantify, such as heating surface conditions, water chemistry, etc.

3) Including the effect of flow regimes explicitly would make the analysis unnecessarily complicated.

This situation is similar to that where velocity profiles are not explicitly treated, but affect the correlation for the slip ratio. Flow regimes will similarly make their effects felt by influencing parameters utilized in empirical correlations.

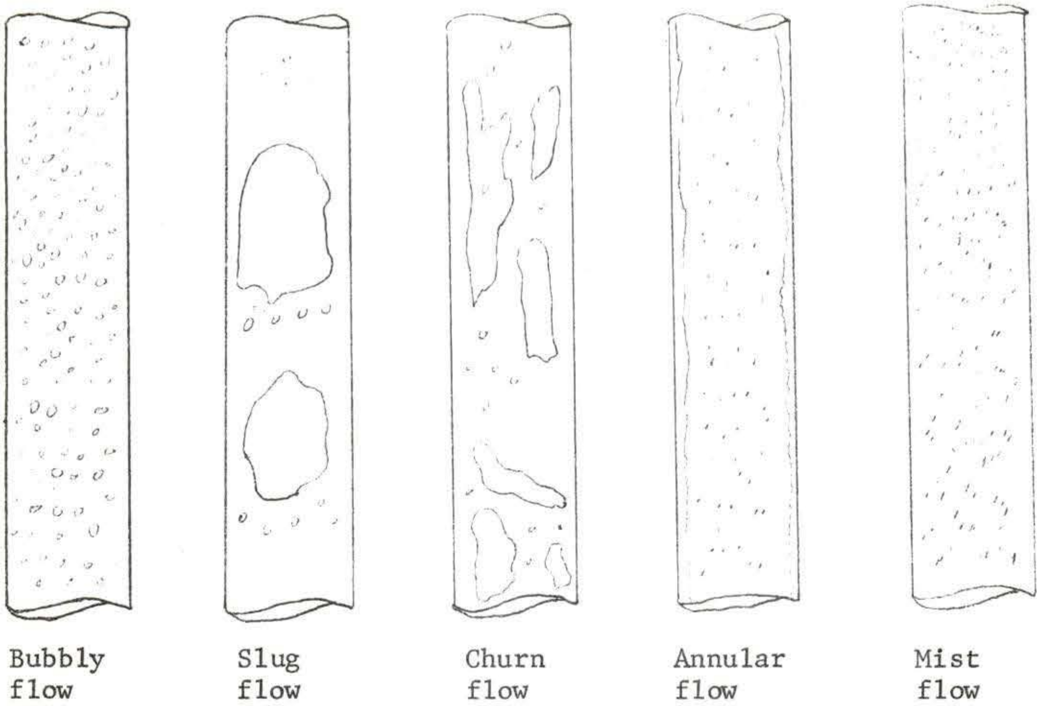

Figure 3.1. Typical flow regime patterns

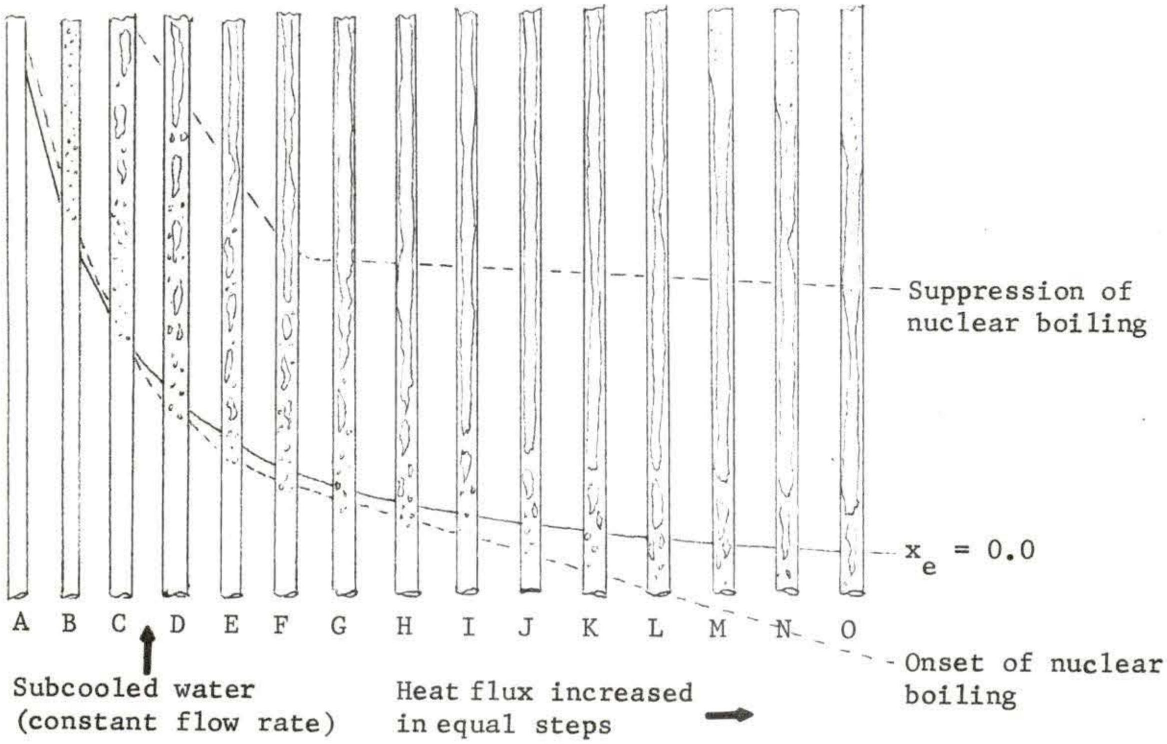

Figure 3.2. Diabatic flow regimes [4]

F. Void-Quality Relation Including Slip Ratio Correlation

The explicit void fraction-quality relationship chosen for use in this study is:

$$\langle\alpha\rangle = \frac{\langle x\rangle}{\left\{C_o\left[\langle x\rangle + \frac{\rho_g}{\rho_\ell}(1 - \langle x\rangle)\right] + \frac{\rho_g V_{gi}}{G}\right\}} \tag{3.27}$$

This is referred to as the Zuber-Findlay void-quality model [4]. Comparing the denominator of the above with the denominator of Equation (3.26) indicates that the correlation for the slip ratio is:

$$S = C_o + \frac{\langle x\rangle(C_o - 1)\rho_\ell}{\rho_g(1 - \langle x\rangle)} + \frac{\rho_\ell V_{gi}}{G(1 - \langle x\rangle)} \tag{3.28}$$

In the above, C_o is a concentration parameter and reflects the tendency of vapor to collect in higher velocity regions in slug flow and annular flow and in turn will be determined from another correlation. V_{gi} is the "drift velocity," a void-weighted velocity of the vapor phase with respect to the velocity of the center of volume of the mixture and defined by:

$$V_{gi} = \frac{\langle\alpha[u_g - j]\rangle}{\langle\alpha\rangle} \tag{3.29}$$

V_{gi} can also be expressed by a correlation. The end effect of these is that the first two terms of Equation (3.28) represent the slip due to the combination of cross-sectional averaging and a nonuniform radial void fraction profile. Together they constitute what is called "integral slip." The last term represents "local slip" between the phases.

The correlation for C_o developed by Dix [3] is:

$$C_o = \langle\beta\rangle\left[1 + \left(\frac{1}{\langle\beta\rangle} - 1\right)^b\right] \qquad (3.30)$$

with

$$b \equiv \left(\frac{\rho_g}{\rho_\ell}\right)^{0.1} \qquad (3.31)$$

If one again considers dividing Equation (3.24) by Equation (3.23):

$$\frac{\langle x\rangle}{1 - \langle x\rangle} = \frac{\rho_g}{\rho_\ell}\,\frac{\langle\beta\rangle}{1 - \langle\beta\rangle} \qquad (3.32)$$

or

$$\langle\beta\rangle = \frac{\langle x\rangle}{\left[(1 - \langle x\rangle)\,\frac{\rho_g}{\rho_\ell} + \langle x\rangle\right]} \qquad (3.33)$$

Thus, if the flow quality is known and (ρ_g/ρ_ℓ) for a particular pressure is known, C_o, for that quality and pressure, can be computed. C_o as a function of $\langle x\rangle$ and pressure can be seen in Figure 3.3.

The correlation for V_{gi} suggested by Lahey [4] as being relatively valid regardless of flow regime is:

$$V_{gi} = 2.9\left[\frac{(\rho_\ell - \rho_g)\sigma g g_c}{\rho_\ell^2}\right]^{1/4} \sin\theta \qquad (3.34)$$

where σ is the surface tension of water at the operating pressure, g is the acceleration due to gravity, g_c is a gravitational conversion factor equal to 32.2 $\frac{\text{lb}_m\text{-ft}}{\text{lb}_f\text{-sec}^2}$, and θ is the angle between the horizontal and the direction of flow. The surface tension as a function of saturation temperature is shown in Table 3.1 based on data from Holman [7]. These are the correlations necessary for calculating the desired void fraction profile.

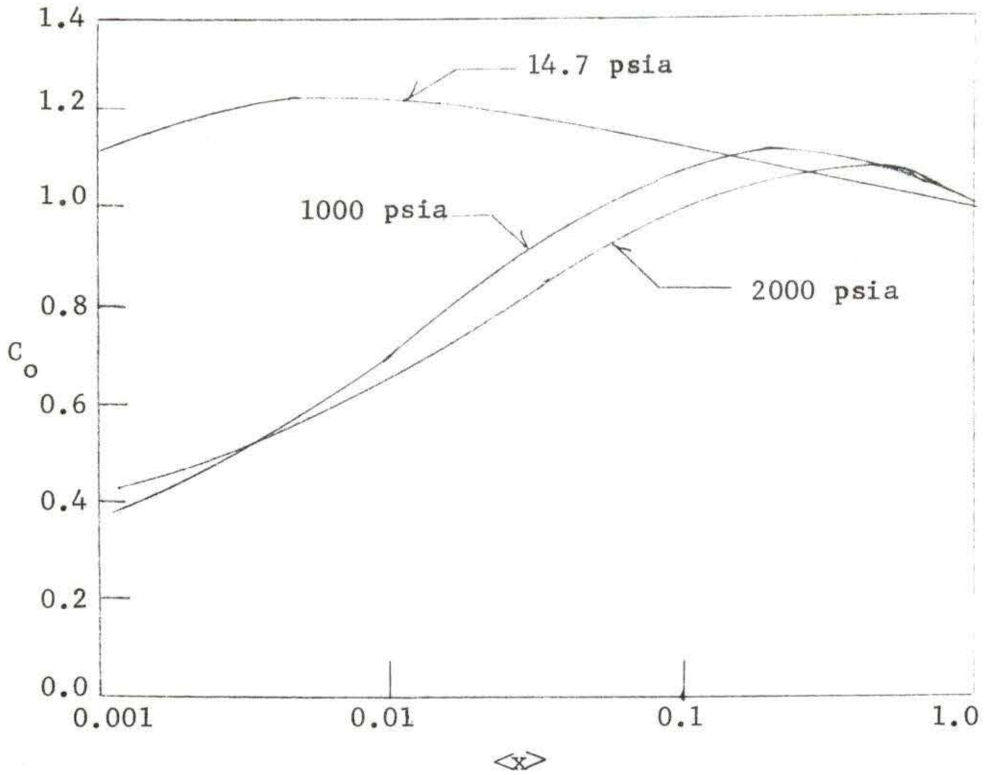

Figure 3.3. Variation of C_o with pressure and flow quality [4]

G. Difference between Bulk and Subcooled Boiling

Finally, it is to be noted that subcooled boiling and bulk boiling are to be treated somewhat differently. In both cases, the same correlation between quality and void fraction, Equation (3.27), is used. The difference lies in determining the flow quality $\langle x \rangle$. Flow quality and the thermodynamic equilibrium quality are the same for bulk boiling and easy to calculate. More correlations must be introduced, however, to calculate $\langle x \rangle$ for subcooled boiling.

Recall Equation (3.22) had the form:

Table 3.1. Surface tension data for water

Surface tension (10^{-4} lb_f/ft)	Temperature (^oF)
51.8	32
50.2	60
47.8	100
45.2	140
41.2	200
40.3	212
31.6	320
21.9	440
11.1	560
1.0	680
0	705.4

$$\langle x(z)\rangle = \frac{\langle h(z)\rangle - \langle h_\ell(z)\rangle}{h_g - \langle h_\ell(z)\rangle} \tag{3.22}$$

$\langle h(z)\rangle$ can be calculated in a straightforward manner from Equation (3.19). The problem lies then in calculating $\langle h_\ell(z)\rangle$, or the mean liquid enthalpy during subcooled boiling.

Two general methods are often applied to finding $\langle h_\ell(z)\rangle$. One is a development of an actual mechanistic model attempting to explain subcooled boiling in terms of physical processes occurring and to predict the subcooled boiling profile based on the model. This technique appears relatively successful but is fairly complicated. The second technique consists of proceeding in blissful ignorance of any physical

processes going on and simply using a subcooled boiling profile of a particular mathematical form that seems to agree well with observed experimental data. Because of its attractive relative simplicity, the profile-fit model will be used for this paper.

Two particular mathematical forms are often used:

$$\frac{(h_f - \langle h_\ell \rangle)}{[h_f - (h_\ell)_d]} = \exp\left\{- \left[\frac{\langle h \rangle - (h_\ell)_d}{h_f - (h_\ell)_d}\right]\right\} \tag{3.35}$$

or

$$\frac{(h_f - \langle h_\ell \rangle)}{[h_f - \langle h_\ell \rangle_d]} = 1 - \tanh\left[\frac{\langle h \rangle - (h_\ell)_d}{h_f - (h_\ell)_d}\right] \tag{3.36}$$

where $(h_\ell)_d$ is defined below. It should be noted that both of these forms satisfy two important boundary conditions:

1) $\dfrac{(h_f - \langle h_\ell \rangle)}{[h_f - (h_\ell)_d]} = 1$ when $\langle h_\ell \rangle = (h_\ell)_d$.

2) $\dfrac{(h_f - \langle h_\ell \rangle)}{[h_f - (h_\ell)_d]}$ approaches 0 as $\langle h_\ell \rangle$ approaches h_f and the corresponding commencement of bulk boiling.

Comments about the quantity $[h_f - (h_\ell)_d]$ are also necessary. Recall that h_f is the enthalpy of saturated liquid at the operating pressure. The second enthalpy term, $(h_\ell)_d$, stands for the mean liquid enthalpy at the axial position when "void departure" begins.

To understand what is meant by "void departure," consider Figure 3.4. As subcooled boiling begins, steam bubbles formed tend to cling and travel in a layer along the wall of the heating surface. Eventually, however, enough bubbles are formed so that they are "ejected" into the main subcooled portion of the flow. The few bubbles clinging to the

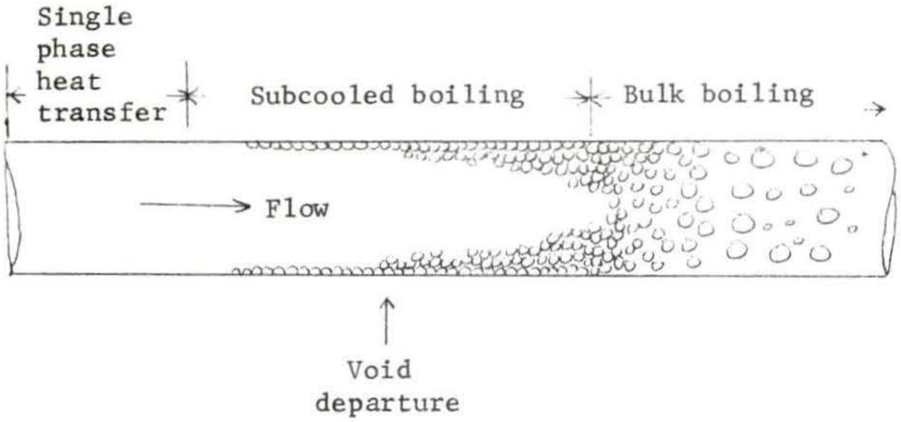

Figure 3.4. Illustration of subcooled boiling

wall constitute an insignificant void fraction and are neglected, but once the "void departure" point when the bubbles are forced into the main stream is reached, the subcooled void fraction becomes significant. Thus, the quantity $[h_f - (h_\ell)_d]$ is the subcooling at void departure or at this point when bubbles begin to be injected into the stream.

One way of determining or estimating $[h_f - (h_\ell)]$ is based on a model developed by Levy in 1966 [4]. Use of the model gives the following relationships:

Let

$$y_b^+ = \frac{0.010(\sigma g_c D_H \rho_f)^{1/2}}{\mu_f} \tag{3.37}$$

Then, if $0 \leq y_b^+ \leq 5.0$:

$$h_f - (h_\ell)_d = C_{P\ell} \frac{q''}{H_{1\phi}} - \frac{q''}{G\sqrt{f/8}} \Pr y_b^+ \tag{3.38}$$

If $5.0 \leq y_b^+ \leq 30.0$:

$$h_f - (h_\ell)_d = C_{P\ell} \frac{q''}{H_{1\phi}} - \frac{5.0\ q''}{G\sqrt{f/8}} \left\{\Pr + \ell n\left[1 + \Pr\left(\frac{y_b^+}{5.0} - 1.0\right)\right]\right\} \tag{3.39}$$

If $y_b^+ \geq 30.0$:

$$h_f - (h_\ell)_d = C_{P\ell}\,\frac{q''}{H_{1\phi}} - \frac{5.0\,q''}{G\sqrt{f/8}}\left\{\mathrm{Pr} + \ell n[1.0 + 5.0\ \mathrm{Pr}] + 0.5\,\ell n\left[\frac{y_b^+}{30.0}\right]\right\} \tag{3.40}$$

In the above, the following variables have not been defined previously in this paper:

D_H = hydraulic diameter = $\dfrac{4(\text{area of duct cross section})}{\text{Wetted perimeter}}$

$\rho_f = \rho_\ell$ = density of liquid phase

μ_f = dynamic viscosity of the liquid phase

$C_{P\ell}$ = specific heat of the liquid phase

q'' = heat flux being added

$H_{1\phi}$ = heat transfer coefficient for single-phase heat transfer

f = friction factor

Pr = Prandtl number.

Thus, using the above relationships, one can estimate the void-departure-subcooling for use in either Equation (3.35) or Equation (3.36).

All of the relationships for calculating a fairly accurate axial void fraction profile have now been introduced. Following is a short summary of the method or "recipe" for calculating the void profile.

H. Void Fraction Profile "Recipe"

Void fraction profile calculational scheme:

Step #1 — Calculate the void departure subcooling from Equation (3.37) and one of Equations (3.38), (3.39), or (3.40).

Step #2 — Calculate $\langle h(z)\rangle$ using Equation (3.19).

Step #3 – Calculate $\langle h_\ell(z)\rangle$ using one of Equations (3.35) or (3.36).

Step #4 – Calculate $\langle x(z)\rangle$ using Equation (3.22). Note that $\langle x(z)\rangle$ will become equal to $\langle x_e(z)\rangle$ for bulk boiling.

Step #5 – Calculate V_{gi} using Equation (3.34).

Step #6 – Calculate b using Equation (3.31).

Step #7 – Calculate $\langle \beta(z)\rangle$ using Equation (3.33).

Step #8 – Calculate $C_o(z)$ using Equation (3.30).

Step #9 – Calculate $\langle \alpha(z)\rangle$ using Equation (3.27).

A numerical example of this procedure using the parameters for the DAEC BWR which operates at a saturation temperature of 547 °F and a nominal pressure of 1020 psia will now be presented: (These parameters may be found in steam tables and in references including the thermal properties of water.)

Step #1 – Equation (3.37) is:

$$y_b^+ = \frac{0.010(\sigma g_c D_H \rho_f)^{1/2}}{\mu_f}$$

$$\sigma \cong 12.2 \times 10^{-4}\ \mathrm{lb_f/ft}$$

$$\rho_f \cong 46.5\ \mathrm{lb_m/ft^3}$$

$$g_c = 32.2\ \frac{\mathrm{lb_m\text{-}ft}}{\mathrm{lb_f\text{-}sec^2}}$$

$$\mu_f \cong 0.230\ \mathrm{lb_m/hr\ ft}$$

$$D_H = \frac{(4)(49)(2.053 \times 10^{-3}\ \mathrm{ft^2})}{(28)(0.738\ \mathrm{in})(1\ \mathrm{ft}/12\ \mathrm{in}) + (49)(2\pi)(0.2815\ \mathrm{in})(1\ \mathrm{ft}/12\ \mathrm{in})}$$

$$= 0.0450\ \mathrm{ft}$$

Note in the above that the hydraulic diameter is calculated using the cross section of an entire 49-fuel element fuel bundle as the "duct cross section." Using the above values gives:

$$y_b^+ = 44.87$$

Thus, Equation (3.40) from Levy's model is appropriate:

$$h_f - (h_\ell)_d = C_{P\ell} \frac{q''}{H_{1\phi}} - \frac{5.0\ q''}{G\sqrt{f/8}} \left\{ Pr + \ell n[1.0 + 5.0\ Pr] + 0.5\ \ell n\left[\frac{y_b^+}{30.0}\right]\right\}$$

These additional physical parameter values are needed:

$$C_{P\ell} \cong 1.34\ \text{Btu/lb}_m{}^\circ\text{F}$$

$$G \cong 1.36 \times 10^6\ \frac{\text{lb}_m}{\text{hr ft}^2}$$

$$Pr \cong = 0.958$$

$$h_f = 545.6\ \frac{\text{Btu}}{\text{lb}_m}$$

$$q'' = (2.69 \times 10^5\ \frac{\text{Btu}}{\text{hr ft}^2}) \sin \frac{\pi z}{12\ \text{ft}}$$

Also, assume a representative value for a single-phase heat transfer coefficient is 5000 $\frac{\text{Btu}}{\text{hr ft}^2}$, so that $H_{1\phi} = 5000\ \frac{\text{Btu}}{\text{hr ft}^2}$. To get a representative value for f, one may calculate the Reynolds number from $Re = \frac{VD_H\rho}{\mu} = \frac{GD_H}{\mu}$ and then consult a Moody diagram for smooth pipes. Doing so gives:

$$Re = \frac{(1.36 \times 10^6\ \frac{\text{lb}_m}{\text{hr ft}^2})(0.0450\ \text{ft})}{0.230\ \frac{\text{lb}_m}{\text{hr ft}}} = 2.66 \times 10^5$$

Then, from a Moody diagram, $f \cong 0.0145$. Finally, note that since $q''(z)$ is a sinusoid rather than a constant value, there are essentially two unknowns in Equation (3.40). One is z_d, the departure point, and the other is $[h_f - (h_\ell)_d]$, the void departure subcooling. To solve this, assume that $(h_\ell)_d \cong \langle h \rangle_d$, which would be given by Equation (3.19):

$$\langle h \rangle = h_{in} + \frac{1}{GA_{CS}} \int_0^z q'dz$$

$$h_{in} = 526.9 \frac{\text{Btu}}{\text{lb}_m}$$

$$GA_{CS} = 2800 \frac{\text{lb}_m}{\text{hr}}$$

$$q' = (3.95 \times 10^4 \frac{\text{Btu}}{\text{hr ft}}) \sin \frac{\pi z}{12 \text{ ft}}$$

Thus:

$$\langle h \rangle_d = 526.9 \frac{\text{Btu}}{\text{lb}_m} + \frac{1}{2800 \text{ lb}_m/\text{hr}} \int_0^{z_d} (3.95 \times 10^4 \frac{\text{Btu}}{\text{hr ft}}) \sin \frac{\pi z}{12 \text{ ft}} dz$$

$$= 580.8 \frac{\text{Btu}}{\text{lb}_m} - (53.9 \frac{\text{Btu}}{\text{lb}_m}) \cos \frac{\pi z_d}{12 \text{ ft}}$$

When this is substituted into Equation (3.40), the net result is:

$$545.6 \frac{\text{Btu}}{\text{lb}_m} - \left[580.8 \frac{\text{Btu}}{\text{lb}_m} - (53.9 \frac{\text{Btu}}{\text{lb}_m}) \cos \frac{\pi z_d}{12 \text{ ft}}\right]$$

$$= (1.34 \frac{\text{Btu}}{\text{lb}_m \, {}^oF}) \left(\frac{(2.69 \times 10^5 \frac{\text{Btu}}{\text{hr ft}^2}) \sin \frac{\pi z_d}{12 \text{ ft}}}{5000 \frac{\text{Btu}}{\text{hr ft}^2}} \right)$$

$$- \frac{(1.345 \times 10^6 \frac{\text{Btu}}{\text{hr ft}^2}) \sin \frac{\pi z_d}{12 \text{ ft}}}{(1.36 \times 10^6 \frac{\text{lb}_m}{\text{hr ft}^2}) \sqrt{\frac{0.0145}{8}}} \left\{0.958 + \ell n(5.79) + \frac{1}{2} \ell n(1.50)\right\}$$

Solving this expression, which includes the assumption that $(h_\ell)_d \approx \langle h \rangle_d$, by iteration gives $z_d \cong 3.0$ ft and $[h_f - (h_\ell)_d] \cong 3.0$ Btu/lb_m.

Step #2 — Equation (3.19) is:

$$\langle h(z)\rangle = h_{in} + \frac{1}{GA_{CS}}\int_0^z q'dz$$

or

$$\langle h(z)\rangle = 526.9\ \frac{Btu}{lb_m} + \frac{1}{2800\ \frac{lb_m}{hr}}\int_0^z \left(3.95 \times 10^4\ \frac{Btu}{hr\ ft}\right)\sin\frac{\pi z}{12\ ft}\,dz$$

or

$$\langle h(z)\rangle = 580.8\ \frac{Btu}{lb_m} - \left(53.9\ \frac{Btu}{lb_m}\right)\cos\frac{\pi z}{12\ ft}$$

Step #3 — Equation (3.35) may be used to calculate $\langle h_\ell(z)\rangle$:

$$\frac{h_f - \langle h_\ell(z)\rangle}{[h_f - (h_\ell)_d]} = \exp\left\{-\left[\frac{\langle h(z)\rangle - (h_\ell)_d}{h_f - (h_\ell)_d}\right]\right\}$$

or

$$\frac{545.6\ \frac{Btu}{lb_m} - \langle h_\ell(z)\rangle}{3.0\ \frac{Btu}{lb_m}} = \exp\left\{-\left(\frac{\langle h(z)\rangle - 542.6\ \frac{Btu}{lb_m}}{3.0\ \frac{Btu}{lb_m}}\right)\right\}$$

Step #4 — Equation (3.22) is:

$$\langle x(z)\rangle = \frac{\langle h(z)\rangle - \langle h_\ell(z)\rangle}{h_g - \langle h_\ell(z)\rangle}$$

or

$$\langle x(z)\rangle = \frac{\langle h(z)\rangle - \langle h_\ell(z)\rangle}{1192.2\ \frac{Btu}{lb_m} - \langle h_\ell(z)\rangle}$$

Step #5 — Equation (3.34) is:

$$V_{gi} = 2.9\left[\frac{(\rho_\ell - \rho_g)\sigma g g_c}{\rho_\ell^2}\right]^{1/4} \sin\theta$$

The following values for parameters above may be used:

$$\rho_{\ell} = 46.5\ \mathrm{lb_m/ft^3}$$

$$g_c = 32.2\ \frac{\mathrm{lb_m\text{-}ft}}{\mathrm{lb_f\text{-}sec^2}}$$

$$g \cong 32.2\ \mathrm{ft/sec^2}$$

$$\sigma \cong 12.2 \times 10^{-4}\ \mathrm{lb_f/ft}$$

$$\rho_g = 2.37\ \mathrm{lb_m/ft^3}$$

$$\sin\theta = 1$$

Then

$$V_{gi} = 2.9\left[\frac{(44.1\ \frac{\mathrm{lb_m}}{\mathrm{ft^3}})(12.2 \times 10^{-4}\ \frac{\mathrm{lb_f}}{\mathrm{ft}})(32.2\ \frac{\mathrm{ft}}{\mathrm{sec^2}})(32.2\ \frac{\mathrm{lb_m\text{-}ft}}{\mathrm{lb_f\text{-}sec^2}})}{(46.5\ \frac{\mathrm{lb_m}}{\mathrm{ft^3}})^2}\right]^{1/4} \quad (1)$$

$$= 1.16\ \frac{\mathrm{ft}}{\mathrm{sec}}$$

<u>Step</u> <u>#6</u> — Equation (3.31) is:

$$b = (\rho_g/\rho_{\ell})^{0.1}$$

$$= (2.37/46.5)^{0.1}$$

$$= 0.743$$

<u>Step</u> <u>#7</u> — Equation (3.33) is:

$$\langle\beta(z)\rangle = \frac{\langle x(z)\rangle}{(1 - \langle x(z)\rangle)\ \frac{\rho_g}{\rho_{\ell}} + \langle x(z)\rangle}$$

or

$$\langle\beta(z)\rangle = \frac{\langle x(z)\rangle}{[(1 - \langle x(z)\rangle)0.051 + \langle x(z)\rangle]}$$

or

$$\langle\beta(z)\rangle = \frac{\langle x(z)\rangle}{0.051 + 0.949\langle x(z)\rangle}$$

<u>Step #8</u> – Equation (3.30) is:

$$C_o(z) = \langle\beta(z)\rangle \left[1 + \left(\frac{1}{\langle\beta(z)\rangle} - 1\right)^b\right]$$

or

$$C_o(z) = \langle\beta(z)\rangle \left[1 + \left(\frac{1}{\langle\beta(z)\rangle} - 1\right)^{0.743}\right]$$

<u>Step #9</u> – Equation (3.27) is:

$$\langle\alpha(z)\rangle = \frac{\langle x(z)\rangle}{\left\{C_o(z)\left[\langle x(z)\rangle + \frac{\rho_g}{\rho_\ell}\,(1 - \langle x(z)\rangle)\right] + \frac{\rho_g V_{gi}}{G}\right\}}$$

or

$$\langle\alpha(z)\rangle = \frac{\langle x(z)\rangle}{C_o(z)[\langle x(z)\rangle + 0.051(1 - \langle x(z)\rangle)] + 0.00728}$$

In Table 3.2 is included data for axial profiles for $\langle h(z)\rangle$, $\langle h_\ell(z)\rangle$, $\langle x(z)\rangle$, $\langle\beta(z)\rangle$, $C_o(z)$, and $\langle\alpha(z)\rangle$.

Table 3.2. Axial variation of calculated parameters used to determine void fraction profile

z (ft)	$\langle h(z)\rangle (\frac{Btu}{lb_m})$	$\langle h_\ell(z)\rangle (\frac{Btu}{lb_m})$	$\langle x(z)\rangle$	$\langle \beta(z)\rangle$	$C_o(z)$	$\langle \alpha(z)\rangle$
1.0	528.7	528.7	0.00×10^{-4}	0.00×10^{-3}	0.00×10^{-1}	0.00×10^{-2}
2.0	534.1	534.1	0.00×10^{-4}	0.00×10^{-3}	0.00×10^{-1}	0.00×10^{-2}
3.0	542.7	542.7	0.00×10^{-4}	0.00×10^{-3}	0.00×10^{-1}	0.00×10^{-2}
3.1	543.7	543.52	2.77×10^{-4}	5.41×10^{-3}	2.66×10^{-1}	1.33×10^{-2}
3.2	544.7	544.11	9.10×10^{-4}	1.76×10^{-2}	3.67×10^{-1}	4.61×10^{-2}
3.3	545.8	544.57	1.90×10^{-3}	3.60×10^{-2}	4.50×10^{-1}	6.12×10^{-2}
3.4	546.9	544.88	3.12×10^{-3}	5.79×10^{-2}	5.18×10^{-1}	8.86×10^{-2}
3.5	548.0	545.10	4.48×10^{-3}	8.11×10^{-2}	5.74×10^{-1}	1.15×10^{-1}
4.0	553.9	545.53	1.28×10^{-2}	2.03×10^{-1}	7.64×10^{-1}	2.31×10^{-1}
5.0	566.8	545.60	3.28×10^{-2}	4.00×10^{-1}	9.41×10^{-1}	3.88×10^{-1}
6.0	580.8	545.6	5.44×10^{-2}	5.30×10^{-1}	1.01×10^{0}	4.91×10^{-1}
7.0	594.8	545.6	7.61×10^{-2}	6.18×10^{-1}	1.05×10^{0}	5.57×10^{-1}
8.0	607.8	545.6	9.62×10^{-2}	6.76×10^{-1}	1.07×10^{0}	6.03×10^{-1}
9.0	618.9	545.6	1.13×10^{-1}	7.15×10^{-1}	1.08×10^{0}	6.35×10^{-1}
10.0	627.5	545.6	1.27×10^{-1}	7.40×10^{-1}	1.08×10^{0}	6.59×10^{-1}

Table 3.2. Continued

z (ft)	$\langle h(z)\rangle (\frac{Btu}{lb_m})$	$\langle h_\ell(z)\rangle (\frac{Btu}{lb_m})$	$\langle x(z)\rangle$	$\langle \beta(z)\rangle$	$C_o(z)$	$\langle \alpha(z)\rangle$
11.0	632.9	545.6	1.35×10^{-1}	7.54×10^{-1}	1.08×10^{0}	6.73×10^{-1}
12.0	634.7	545.6	1.38×10^{-1}	7.58×10^{-1}	1.08×10^{0}	6.77×10^{-1}

IV. DESCRIPTION OF COMPUTER PROGRAMS UTILIZED

A. Introduction

Two different computer programs, LEOPARD and FOG, are utilized in this study. LEOPARD, an acronym for Lifetime Evaluating Operations Pertinent to the Analysis of Reactor Designs, is used to obtain few group macroscopic cross sections from input data such as the unit cell composition, fuel temperature, cladding temperature, moderator temperature, moderator void fraction, reactor pressure, etc. These macroscopic cross sections are then used as input data to FOG. FOG is a one-dimensional neutron diffusion code with the capability of calculating one-dimensional neutron flux profiles and of performing a variety of criticality searches.

B. General Multigroup Method

A great many of the nuclear parameters utilized in nuclear engineering are functions of the energy of the neutrons involved. Cross sections for various types of nuclear reactions, such as scattering, absorption, and fission, are often very sensitive to neutron energy, particularly near resonance peaks. Representing these cross sections as explicit mathematical functions of energy is usually impossible. Instead, the energy range of interest is divided into a large number of small intervals, and the cross section data within each of these "fine mesh" intervals is stored in a "library." Thus, there would be a library for each isotope and for each reaction of interest. When a macroscopic cross section for a certain isotope and reaction is needed, this fine mesh data can be coalesced into data for just a few groups, such as one thermal group and one fast group or one thermal group and three fast groups. The above technique is called a multigroup method of approaching the problem. Probably the other major way of handling this problem is to use Monte Carlo techniques, which unfortunately often become quite expensive. The multigroup data utilized in LEOPARD includes the 54 fast group cross section data and the 172 thermal group cross sections from MUFT-5 [8] and KATE-1 [9] respectively. KATE-1 and MUFT-5 are both codes developed by Westinghouse, as is LEOPARD.

Obtaining few group macroscopic cross sections is just the beginning of the multigroup method. The second major endeavor is to determine flux profiles and corresponding k-eigenvalues. This may be done by solving a multigroup diffusion equation of the form:

$$- D^i \nabla^2 \phi^i + \Sigma_T^i \phi^i = x^i s(r) + \Sigma_{s,(i-1)\to i} \phi^{(i-1)} \tag{4.1}$$

The symbols are defined as:

ϕ^i = neutron flux in the ith group

D^i = diffusion constant for the ith group

Σ_T^i = total removal for the ith group

$= D^i (B^2)^i + \Sigma_a^i + t^p \Sigma_p^{th} + \Sigma_{s,i\to(i+1)}$

where

$(B^2)^i$ = transverse buckling for the ith group

Σ_a^i = absorption cross section for the ith group

Σ_p^{th} = poison cross section in the thermal group

t^p = ratio of poison cross section in group i to thermal poison cross section

$\Sigma_{s,i\rightarrow j}$ = scattering or transfer coefficient from group i to group j

x^i = the integral of the fission spectrum over the lethargy range represented by group i

r = distance measured from the origin

$\nabla^2 = d^2/dr^2 + P/r\, d\phi/dr$ (P = 0 in plane geometry; P = 1 in cylindrical geometry; P = 2 in spherical geometry)

s = normalized source density

$$= \sum_{i=1}^{NOG} \frac{(\nu\Sigma_f)^i \phi^i}{\lambda}$$

where

NOG = number of groups

Σ_f^i = the fission cross section in the ith group

ν^i = the average number of neutrons produced by a fission in the ith group

λ = the eigenvalue, which is related to the multiplication factor k

These coupled differential equations are then solved by an iterative process which continues until the solution converges.

This, then, is a very general sketch of the multigroup method and its use with diffusion theory. Next, consider the codes LEOPARD and FOG a little more closely. Note that LEOPARD and FOG are chosen for use in this study because they are already available and in use here at Iowa State University.

C. The LEOPARD Code

Good discussions of the various approximations utilized and the neutron physics involved in LEOPARD appear in the 1973 Ph.D. dissertation by Crudele [10] and in the Westinghouse report by Strawbridge [11]. For the purposes of this study, however, more attention will be focused upon the use of LEOPARD than upon its theoretical basis.

Input data for LEOPARD is determined by looking at a unit cell of the reactor lattice. Recall that a unit cell is the repeating unit or basic "building block" of the lattice and consists of a cylindrical fuel pellet, the surrounding cladding, and a portion of the moderator-coolant "allocated" to that particular fuel pin. Because dimensions usually remain constant along the vertical axis of the core, unit cells are based on a cross-sectional view of the lattice geometry. Some typical geometries are square and hexagonal, so that the unit cells appear as in Figure 4.1 and Figure 4.2. BWR's usually have square lattices. Note that the fuel region has been shown as a cylindrical fuel pellet, but modifications by Kim [12] of LEOPARD make it possible to treat plate-type fuel elements and the associated geometry.

The three regions of the unit cell listed above are the fuel pellet, the cladding, and the moderator. If a gap exists between the fuel pellet and the cladding jacket, the input data can reflect this so that it will be appropriately treated by LEOPARD. Often a significant fraction of a reactor core is occupied by water slots, fuel assembly walls or cans, control rod followers, and/or structural materials. LEOPARD handles this by defining a fourth fictitious "extra" region

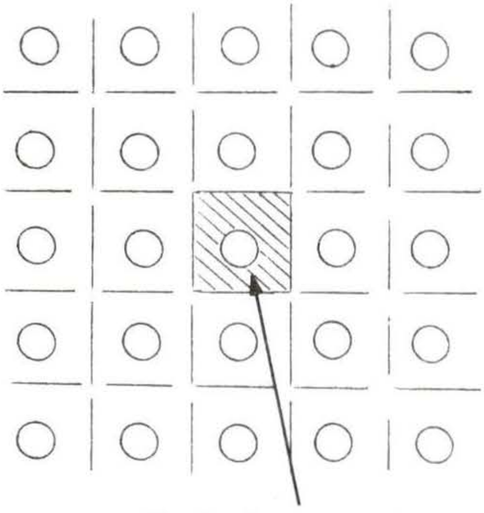

Figure 4.1. Unit cells for square lattice

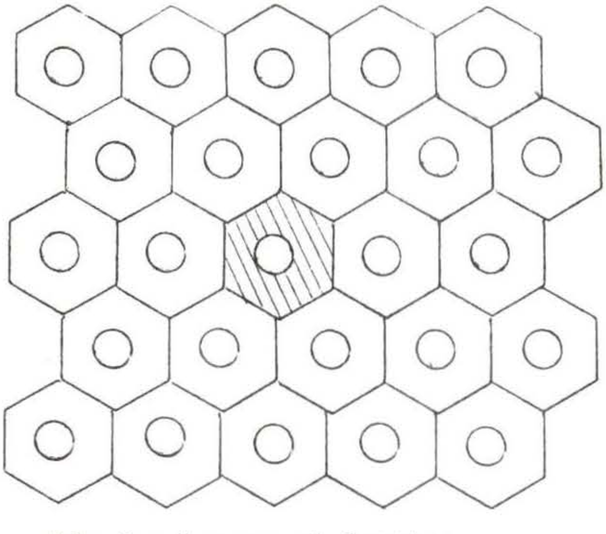

Figure 4.2. Unit cells for hexagonal lattice

and adding this to the three "real" regions to form a "super cell." The calculation of parameters such as D, Σ_a, Σ_f, etc. is then based on the volumetric composition of each of these four regions in the super cell and on the volume fraction of the total core occupied by "extra" regions.

LEOPARD calculates these group parameters by assuming a homogeneous reactor having the same volumetric fraction of each element or material as that indicated in the input data for the unit cell. Although the reactor is in truth heterogeneous, this homogeneous treatment yields good results for heterogeneous reactor cores having many fuel elements, as do power reactors [13].

A numerical example of the unit cell volumetric composition is in order at this point. Consider the unit cell for the DAEC BWR shown in Figure 4.3. The volumetric compositions of the pellet, cladding, and moderator regions are:

Pellet — 100% of UO_2
Cladding — 87.04% of zircaloy-4
Moderator — (100% - void fraction) of H_2O

Note that the cladding region is considered to be 87% zircaloy and the remainder to be a gap between the pellet and cladding. LEOPARD automatically computes the size of this gap when the data is entered in the above fashion. Finally, note that the moderator may include steam bubbles having no moderating power, so that the volume fraction entered is that occupied by the liquid phase of the steam-water mixture. Also note that the 87% figure for the volume fraction of zircaloy in the cladding region arises from the calculation based on dimensions shown in Figure 4.3:

$$\frac{\pi(0.2815\ \text{in})^2 - \pi(0.2445\ \text{in})^2}{\pi(0.2815\ \text{in})^2 - \pi(0.2385\ \text{in})^2} = 0.8704 \qquad (4.2)$$

But what about the "extra" region needed for the super cell? To obtain data for this, one needs to consider the geometry shown in Figure 4.4.

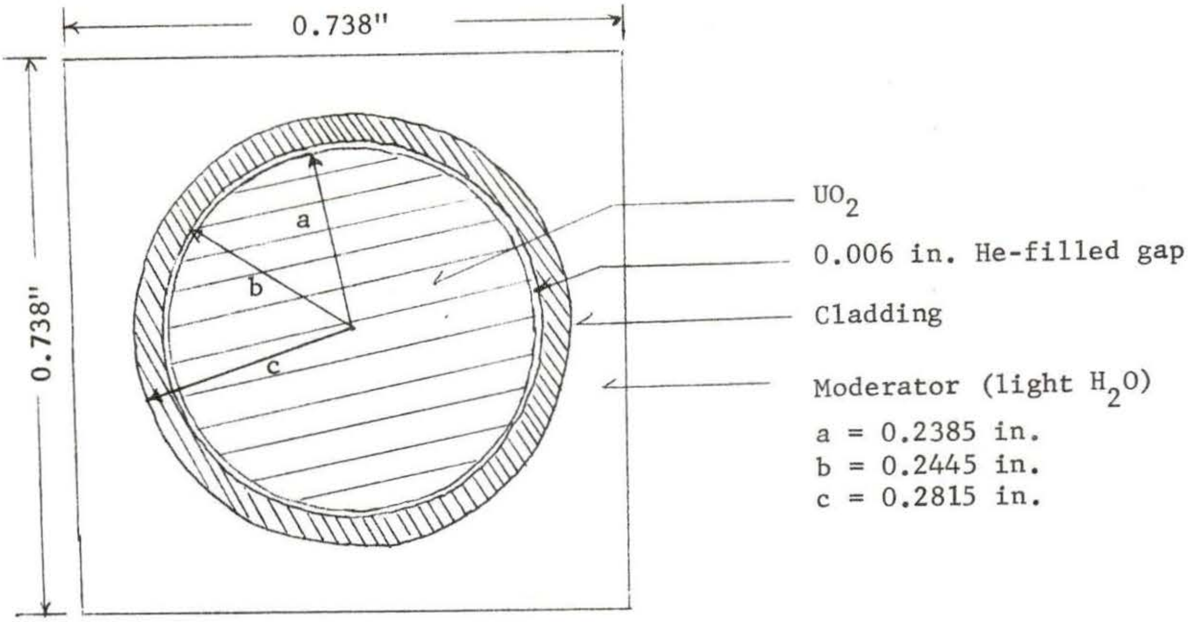

Figure 4.3. DAEC BWR unit cell

There are 49 fuel pins in each fuel bundle for the DAEC BWR and one cruciform-shaped control rod for each four fuel bundles. The control rod travels between the fuel channel walls of the four bundles.

One may first calculate the nonlattice fraction from:

$$\frac{144\ \text{in}^2 - (4)(49)(0.738\ \text{in})^2}{144\ \text{in}^2} = 0.2587 \tag{4.3}$$

If one then considers the extra region when the control rod is withdrawn, it will consist of water filling the spaces between the zircaloy-2 walls of the buel bundles. The volume fraction occupied by the channel walls will be approximately:

$$\frac{4 \times (4)(5.278\ \text{in})(0.08\ \text{in})}{(0.2587)(144\ \text{in}^2)} = 0.181 \tag{4.4}$$

The remaining volume fraction of the extra region, or 0.819, would then be water.

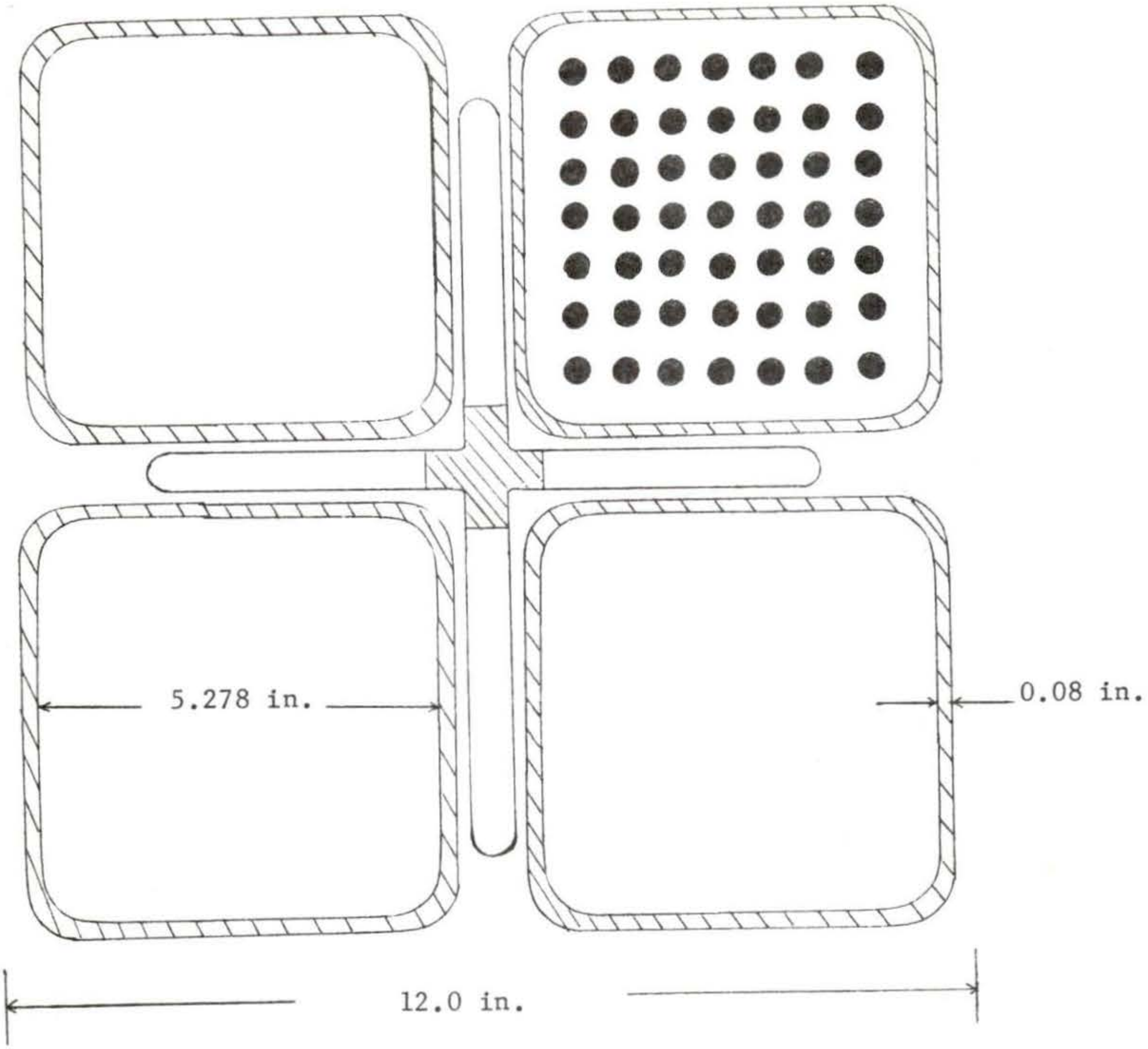

Figure 4.4. Geometry of four fuel bundles

When the super cell composition data is entered on cards, one element or material, identified by an index number, is entered with its volumetric fraction in each of the four regions on a single card. These index numbers appear in WCAP-3269-26 [14], a report explaining the use of LEOPARD, and also in Table 4.1.

In some cases, it may not be possible to determine the volume fraction of an important isotope. Uranium-235 is a good example of

Table 4.1. Index of elements and compounds for LEOPARD

Index #	Element or compound	Index #	Element or compound
1	H	27	Xe-135
2	O	28	Fission products
3	Zircaloy-2	29	B-10
4	C	38	D
6	Fe	50	U-233
7	Ne	51	U-234
9	Al	62	Th-232
11	Cr	65	Pa-233
15	Mn	75	Pr-149
18	U-235	97	ThO_2
19	U-236	98	PuO_2
20	U-238	99	UO_2
21	Pu-239	100	H_2O
22	Pu-240	101	D_2O
23	Pu-241	304	Stainless steel-304
24	Pu-242	316	Stainless steel-316
25	I-135	348	Stainless steel-348
26	Sm-149		

this, since only the enrichment fraction is known. Elements or compounds for which volume fraction data cannot be used are referred to as "trace elements" and their weight fraction or atom fraction is entered instead.

Thus, the data cards for the DAEC BWR cell composition would be:

Index #	Pellet	Clad	Moderator	"Extra"	(Explanation)
99	1.0	0.0	0.0	0.0	(99 = UO_2)
100	0.0	0.0	1.0	0.819	(100 = H_2O)
3	0.0	0.8704	0.0	0.181	(3 = zircaloy)
777	0.0	0.0	0.0	0.0	
18	- 0.01875				(18 = U^{235})
777	0.0	0.0	0.0	0.0	

The "-" sign for the U^{235} entry indicates that a weight fraction is being entered. Note that "777" cards separate "trace element" entries from volume fraction entries and also separate cell composition data from other data entered for LEOPARD. The above example is for no steam bubbles in the moderator. If there was a void fraction of 40%, the second card would become:

100	0.0	0.0	0.6	0.819

Other information besides cell composition data must be entered in LEOPARD. This includes the reactor pressure, dimensions of the unit cell, buckling, the percentage of the theoretical density of UO_2 of the fuel pellets, and temperatures for the fuel pellet, cladding, and moderator. A large part of this information is needed to compute atomic densities at operating pressures and temperatures and to correct microscopic cross section values for temperature effects. Thus, knowledge of approximate axial temperature profiles in the fuel, cladding, and moderator is needed to complete the data needed for LEOPARD. The development of these profiles is treated in another section of this study. Next consider some of the features of the FOG code.

D. The FOG Code

As mentioned previously, FOG computes one-dimensional flux profiles in planar, cylindrical, or spherical geometry by solving Equation (4.1) in an iterative fashion. Between one and four energy groups may be used, but slowing down is permitted only from one energy group to the next lowest energy group. Up to 40 different spatial regions, each region having different values for D, Σ_a, $\nu\Sigma_f$, etc. may be used, with the total number of mesh points not exceeding 239. Boundary conditions that may be chosen include zero flux, zero current, fixed flux, or an extrapolated boundary. The finite difference approximations to derivatives and the manner in which boundary conditions are handled in FOG have been treated extensively by Munson [15].

In addition to its capability to compute flux profiles and also to compute reactivities, FOG has options for performing several "criticality searches." In these searches, the value of a selected parameter is varied until a certain eigenvalue is reached. Often the eigenvalue is 1.0, corresponding to a critical reactor. The search options are:

1) Vary the value of the transverse buckling in particular regions or over the entire reactor

2) Vary the amount of a homogeneous poison (Σ_p) in particular regions or over the entire reactor

3) Vary the dimensions of a particular region or the dimensions of the entire reactor

4) Vary the position of a poison boundary

5) Search on the fuel loading

These last two searches are quite similar. In the fuel loading search, the dividing line between a region with fuel and a region without fuel is moved until there is enough fuel for criticality. In the poison boundary search, the dividing line between a region with poison and a region without poison or between two regions with differing amounts of poison is moved until criticality is obtained. One might think of this as roughly corresponding to the movement of a control rod that has been homogenized with the rest of the reactor materials.

Input data for FOG can be prepared fairly simply by referring to Appendix II in the report by H. P. Flatt [16]. It is to be cautioned, however, that the first alphanumeric card may not be used freely. It must contain one of four entries: FOG2 in columns 1-4, FOG3 in columns 1-4, CLER in columns 45-48, or ENDP in columns 49-52. FOG2 or FOG3 specify options, CLER separates sets of data when more than one reactor configuration is run, and ENDP signifies the last item of input data has been entered. Other alphanumeric information may be entered, but the above entries must appear in the proper positions.

The above are some of the important features of the FOG code. Next, consider how temperature profile data may be obtained.

V. AXIAL TEMPERATURE PROFILES

A. Introduction

Recall that determining realistic macroscopic cross section data utilizing the LEOPARD code requires some knowledge of approximate axial temperature profiles in the fuel, cladding, and moderator so that appropriate values may be included in LEOPARD input data. To obtain this information, the familiar analogy between resistance to heat flow and resistance to the flow of electrical current may be employed. Referring to Figure 5.1, one sees that temperature is analogous to voltage, heat flow is analogous to current, and thermal resistance is analogous to electrical resistance. Solutions of the Poisson heat equation for steady state heat transfer with heat generation and of the Laplace heat equation for steady state heat transfer without heat generation indicate that in cylindrical geometry, thermal resistances of the forms shown below are appropriate.

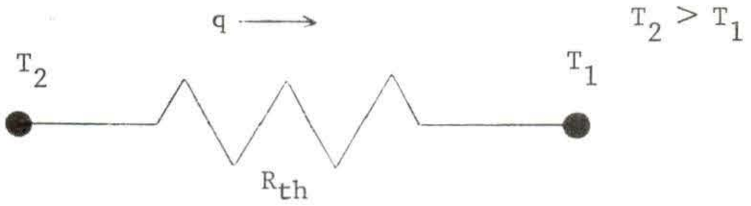

Figure 5.1. Illustration of analogy of electrical current and heat flow

B. Thermal Resistances

1) For the fuel pellet,

$$R_{fuel} = \frac{r_{fuel}}{2k_{fuel}A_{fuel}} \tag{5.1}$$

where

r_{fuel} = radius of the fuel pellet

k_{fuel} = thermal conductivity of the fuel

A_{fuel} = fuel pellet surface area

$= (2\pi)(r_{fuel})(L)$

L = arbitrary length of fuel element

2) For the cladding,

$$R_{cladding} = \frac{r_{cladding}}{k_{cladding}A'_{cladding}} \tag{5.2}$$

where

$r_{cladding}$ = thickness of cladding

$k_{cladding}$ = thermal conductivity of cladding

$A'_{cladding}$ = log mean cladding surface area

$$= (2\pi)\left[\frac{r_{cladding}}{\ell n\left(\frac{r_{fuel} + r_{gap} + r_{cladding}}{r_{fuel} + r_{gap}}\right)}\right](L)$$

$$\cong (2\pi)(r_{fuel} + r_{gap} + \frac{1}{2} r_{cladding})(L)$$

r_{gap} = thickness of any pellet-cladding gap

3) For a pellet-cladding gap,

$$R_{gap} = \frac{r_{gap}}{k_{gap}A'_{gap}} \tag{5.3}$$

where

k_{gap} = thermal conductivity of gas filling gap (usually He)

A'_{gap} = log mean gap surface area

$$= (2\pi)\left[\frac{r_{gap}}{\ell n\left(\frac{r_{fuel} + r_{gap}}{r_{fuel}}\right)}\right](L)$$

$$\cong (2\pi)(r_{\text{fuel}} + \frac{1}{2} r_{\text{gap}})(L)$$

Now, knowledge of the magnitude of each of these three thermal resistance terms enables calculation of temperature differences between the pellet center and the pellet surface, between the pellet surface and the inner cladding surface, and across the cladding. Recalling the unit cell dimensions for the DAEC BWR from Figure 4.3 and taking $k_{\text{fuel}} = 2.42 \frac{\text{Btu}}{\text{hr ft }^{\circ}\text{F}}$ [17], $k_{\text{cladding}} = 9.42 \frac{\text{Btu}}{\text{hr ft }^{\circ}\text{F}}$ [18], and $k_{\text{gap}} = 0.16 \frac{\text{Btu}}{\text{hr ft }^{\circ}\text{F}}$ [19] gives the following:

$$R_{\text{fuel}} = \frac{0.2385 \text{ in}}{(2)(2.42 \frac{\text{Btu}}{\text{hr ft }^{\circ}\text{F}})(2\pi)(0.2385 \text{ in})(1 \text{ ft})} \tag{5.4}$$

$$= 0.0329 \left(\frac{\text{Btu}}{\text{hr }^{\circ}\text{F}}\right)^{-1}$$

$$R_{\text{cladding}} = \frac{0.037 \text{ in}}{(9.42 \frac{\text{Btu}}{\text{hr ft }^{\circ}\text{F}})(2\pi)\left(\frac{0.037 \text{ in}}{\ell n \frac{0.2815 \text{ in}}{0.2445 \text{ in}}}\right)(1 \text{ ft})} \tag{5.5}$$

$$= 0.00238 \left(\frac{\text{Btu}}{\text{hr }^{\circ}\text{F}}\right)^{-1}$$

$$R_{\text{gap}} = \frac{0.006 \text{ in}}{(0.16 \frac{\text{Btu}}{\text{hr ft }^{\circ}\text{F}})(2\pi)\left(\frac{0.006 \text{ in}}{\ell n \frac{0.2445 \text{ in}}{0.2385 \text{ in}}}\right)(1 \text{ ft})} \tag{5.6}$$

$$= 0.0247 \left(\frac{\text{Btu}}{\text{hr }^{\circ}\text{F}}\right)^{-1}$$

Note that L has arbitrarily been taken to be 1.0 ft in the above.

C. Temperature Profiles

The information presented so far only enables the calculation of temperature differences, not temperatures. Thus, to calculate temperatures, one must know the temperature of the outer cladding wall. Where bulk boiling is occurring, this may be estimated from the Jens-Lottes correlation [20]:

$$T_{wall} - T_{sat} = 60\left[\frac{q'}{10^6}\right]^{1/4} e^{-P/900} \tag{5.7}$$

where

T_{sat} = saturation temperature of the coolant

T_{wall} = cladding surface temperature

P = pressure in psia

q' = heat flux in Btu/hr ft^2.

In this study, a fuel bundle representing average conditions in the DAEC BWR is considered. Thus, the linear heat generation rate is:

$$q' = (3.95 \times 10^4 \frac{\text{Btu}}{\text{ft hr}}) \sin \frac{\pi z}{12 \text{ ft}} \tag{5.8}$$

Similarly, the heat flux is:

$$q'' = (2.69 \times 10^5 \frac{\text{Btu}}{\text{hr ft}^2}) \sin \frac{\pi z}{12 \text{ ft}} \tag{5.9}$$

This assumption of a sinusoidal axial power shape agrees well with the axial power distribution shown in Volume 3 of the FSAR for the DAEC reactor [21].

Recall that in Section III a void fraction profile for an average DAEC fuel bundle was determined. From the axial profile of the coolant enthalpy utilized, one may determine an axial coolant bulk temperature profile. For heights above about 5.0 ft, bulk boiling is occurring, T_{sat} has a value of about 547 $^{\circ}$F at 1020 psia, and the Jens-Lottes correlation can be used to estimate the cladding surface temperature.

Putting appropriate values for z into Equation (5.9) and inserting that result in Equation (5.7) produces the results in Table 5.1.

Table 5.1. Cladding surface temperatures for bulk boiling

Axial height (ft)	T_{wall} (^oF)
5.0	560.8
6.0	560.9
8.0	560.4
10.0	558.7
12.0	547.0

Note that, as would be expected from Equation (5.7), T_{wall} is not particularly sensitive to q". For heights less than 5.0 ft, coolant temperatures can be estimated by matching the specific enthalpy values ($\langle\langle h_\ell(z)\rangle\rangle$) calculated in obtaining a void fraction profile in Section III with those of saturated liquid found in steam tables. Even though the coolant is actually subcooled, treating it as saturated liquid is a good approximation here. Results are shown in Table 5.2. To then estimate T_{wall} where single-phase heat transfer is occurring, one may pick a representative heat transfer coefficient and utilize the fact that the thermal resistance term for convective heat transfer is:

$$R_{convection} = \frac{1}{hA_{cladding}} \qquad (5.10)$$

where

h = single phase heat transfer coefficient

Table 5.2. Coolant temperatures in lower core

Axial height (ft)	$T_{coolant}$ (^oF)
0.0	530.0
1.0	533.6
2.0	537.9
3.0	544.7
4.0	547.0

$A_{cladding}$ = outer cladding surface area

Then, using

$$qR_{convection} = T_{wall} - T_{coolant} \tag{5.11}$$

or

$$q'' = h(T_{wall} - T_{coolant}) \tag{5.12}$$

typical cladding surface temperatures in the lower core may be estimated as shown in Table 5.3. An h value of 5000 Btu/hr ft^2 is again used, in order to be consistent with the representative heat transfer coefficient used in the void fraction profile calculation. Again, it should be pointed out that these are estimates rather than precise calculations. Obviously, the temperatures in Table 5.1 and Table 5.3 do not match very well at the boundary between the two regions because to do so, the heat transfer coefficient, h, in (5.12) would need to be expressed as a function of height in the core, since one would expect it to vary as conditions change from those of single phase heat transfer to those of bulk boiling, with the accompanying "pumping action." It is this

Table 5.3. Cladding surface temperatures in lower core

Axial height (ft)	T_{wall} (^oF)
0.0	530.0
1.0	547.5
2.0	560.5
3.0	582.7
4.0	593.6

pumping action that increases the efficiency of heat transfer from the cladding surface to the coolant and thus lowers the thermal resistance.

Once that a satisfactory profile for the cladding surface temperature has been estimated, it is a relatively easy procedure to determine temperatures at the cladding-gap interface, the gap-pellet interface, and the pellet centerline using Equations (5.4), (5.5), and (5.6) in

$$q' = \frac{\Delta T}{R_{th}} \tag{5.13}$$

Results are shown in Table 5.4.

D. Temperatures Used in LEOPARD

All of the temperatures that have been calculated above are those existing either at the pellet center or at interfaces. Because LEOPARD input uses only one temperature for each region, a temperature more characteristic of each material and each axial position chosen needs to be used. A reasonable approach is to use the temperature at radial positions corresponding to the volume-averaged radii of the cylindrical

Table 5.4. Axial temperature profiles

Height from core bottom (ft)	q' $(\frac{\text{Btu}}{\text{hr ft}})$	Coolant temp (^{o}F)	Clad surface temp (^{o}F)	Clad-He interface temp (^{o}F)	He-UO_2 interface temp (^{o}F)	Fuel center temp (^{o}F)
0.0	0.00×10^4	530	530	530	530	530
2.0	1.98×10^4	538	561	608	1100	1750
4.0	3.42×10^4	547	594	676	1520	2650
6.0	3.95×10^4	547	561	655	1630	2930
8.0	3.42×10^4	547	560	642	1490	2610
10.0	1.98×10^4	547	559	606	1100	1750
12.0	0.00×10^4	547	547	547	547	547

fuel pellet and of the surrounding cladding in the unit cell. These positions then mark the "middle" of the fuel and of the cladding. The volume-averaged radii of the pellet and of the cladding for the DAEC BWR are 0.1686 in. and 0.2636 in., respectively. Then, to obtain the fuel temperature in the fuel at a radial position of 0.1686 in. and any axial position, note that the solution to the Poisson equation in cylindrical coordinates is:

$$t - t_1 = \frac{q'''}{4k_{fuel}} (a^2 - r^2) \tag{5.14}$$

where

t = temperature at a radial distance r

a = radius of pellet

t_1 = temperature at $r = a$

q''' = volumetric heat source

k_{fuel} = thermal conductivity of the fuel

From the above, note that the fuel centerline temperature would be:

$$t_{CL} = t_1 + \frac{q'''}{4k_{fuel}} (a^2) \tag{5.15}$$

Combining Equations (5.14) and (5.15) and taking $r = 0.1686$ in. $= 0.01405$ ft gives:

$$t(0.1686 \text{ in.}) = t_{CL} - \frac{q'''}{4k_{fuel}} (0.01405 \text{ ft})^2 \tag{5.16}$$

From Equation (5.16) a fuel temperature suitable for LEOPARD may be calculated for axial positions of interest.

In the cladding, temperature rises are less severe, so that a linear interpolation between the inner and outer cladding surface values for a radial position of 0.2636 in. gives a temperature value suitable for LEOPARD.

In this section, a method of estimating temperatures for use in LEOPARD has been presented. Next, attention will be turned to the results of LEOPARD and FOG applied to a typical BWR core like that of the DAEC BWR.

VI. RESULTS OF COMPUTER-AIDED STUDIES

A. Procedure Used

In this section, LEOPARD and FOG are used to study the axial variation of the ratio of fast flux to thermal flux in a fuel bundle representing average conditions in the DAEC BWR. The spatially continuous axial profiles of temperatures and void fraction are approximated by dividing the 144-inch-long fuel bundle into several shorter segments and using the temperatures and void fraction at the axial position of the midpoint of each of these segments as representative position-independent values within each segment. Variations in the moderator pressure in the axial direction are not considered and a constant value of 1020 psia is used. This information, along with unit cell composition data corresponding to the initial core loading and an average enrichment of 1.875% by weight, is then used as input for the LEOPARD code. No thermal poisons are included in input to LEOPARD, but are included in determination of flux profiles by FOG. Such thermal poisons are usually concentrated in either control rods or in a few gadolinia bearing rods within each fuel bundle. Gadolinia is the burnable poison used by General Electric with the thermal poisoning effect due to neutron capture by Gd^{155} and Gd^{157}. These isotopes constitute 14.9% and 15.7%, respectively, of naturally occurring gadolinium. Gadolinium is included in a few fuel rods in the form of Gd_2O_3 in solid solution with the UO_2 and comprising on the order of 2-3% by weight of the fuel material. Because these materials are concentrated, it would seem that they should not have a large effect upon neutron diffusion parameters, etc. for the rest of the lattice. In addition, the FOG code does have capabilities for including thermal poisons.

B. LEOPARD Data

Input and output of LEOPARD is summarized in Tables 6.1 and 6.2. Some comments about the output are in order. Recall that the neutron energy group referred to by "1" is the fast group, while "2" represents the thermal group. In the numbering of regions, Region 1 is at the bottom of the core and Region 7 is at the top of the core. Regions 2 and 3 are chosen to be shorter segments because it is at a height of about 3 ft that a significant void fraction appears, and this marks an appropriate dividing line between regions. Note that it is the axial variation in the void fraction that probably has the strongest effect on the variation in the parameters calculated by LEOPARD. After values of D, Σ_a, Σ_R, and $\nu\Sigma_f$ have been computed for each of the seven spatial regions and each of the two neutron energy groups, these values become input data for FOG, which computes axial flux profiles.

C. Use of FOG

The primary reason for using FOG is to obtain axial profiles of the fast flux and of the thermal flux. But FOG also includes in its output values for the volume-average flux in each group in each of the spatial regions. Thus, the ratio of fast flux to thermal flux can be calculated using these average values and can be usefully employed

Table 6.1. LEOPARD input data

Region	Axial position of region (ft)	Region midpoint (ft)	Fuel temp (^oF)	Clad temp (^oF)	Moderator temp (^oF)	Void fraction (%)
1	0-2	1.0	990	560	534	0.000
2	2-3	2.5	1620	602	541	0.000
3	3-4	3.5	1960	626	547	0.115
4	4-6	5.0	2220	605	547	0.388
5	6-8	7.0	2220	605	547	0.557
6	8-10	9.0	1780	592	547	0.635
7	10-12	11.0	1000	569	547	0.673

Table 6.2. LEOPARD output data

Region	Neutron energy group	D (cm)	Σ_a (cm^{-1})	Σ_R (cm^{-1})	$\nu\Sigma_f$ (cm^{-1})
1	1	1.462	6.77×10^{-3}	2.10×10^{-2}	4.09×10^{-3}
	2	0.356	5.01×10^{-2}	0.00	7.33×10^{-2}
2	1	1.475	6.88×10^{-3}	2.06×10^{-2}	4.06×10^{-3}
	2	0.361	4.97×10^{-2}	0.00	7.28×10^{-2}
3	1	1.545	6.82×10^{-3}	1.82×10^{-2}	4.02×10^{-3}
	2	0.389	4.87×10^{-2}	0.00	7.21×10^{-2}
4	1	1.710	6.58×10^{-3}	1.47×10^{-2}	3.92×10^{-3}
	2	0.466	4.68×10^{-2}	0.00	7.08×10^{-2}
5	1	1.826	6.35×10^{-3}	1.23×10^{-2}	3.85×10^{-3}
	2	0.529	4.54×10^{-2}	0.00	6.97×10^{-2}
6	1	1.876	6.18×10^{-3}	1.12×10^{-2}	3.82×10^{-3}
	2	0.564	4.49×10^{-2}	0.00	6.93×10^{-2}
7	1	1.893	6.02×10^{-3}	1.08×10^{-2}	3.82×10^{-3}
	2	0.581	4.47×10^{-2}	0.00	6.93×10^{-2}

to observe general trends in the axial variation of the ratio of the fast flux to thermal flux as various conditions change. Next, consider some cases of interest.

The flux profiles corresponding to three different sets of conditions will be of most interest. These cases are:

1) The flux shapes corresponding to the use of LEOPARD-generated cross sections and diffusion constants in a FOG flux calculation without

the addition of any thermal poison whatsoever. This will correspond to a supercritical reactor configuration and thus would not exist under steady-state operating conditions. It is interesting, however, to observe the resulting flux profiles.

2) The flux shapes corresponding to the use of LEOPARD-generated data and the addition of a uniform thermal poison throughout the entire reactor core. This is accomplished by utilizing the second search option listed under the description of the FOG code in Section IV of this study to obtain an eigenvalue of unity.

3) The flux shapes obtained when LEOPARD-generated data is used and varying amounts of thermal poison are introduced in each of the different regions of the reactor. The object of this endeavor is to produce a sinusoidally-shaped thermal flux to correspond to the assumption of a sinusoidal power distribution made when the void fraction profile was calculated in Section III. Again, an eigenvalue of unity is sought, corresponding to a critical reactor.

The flux profiles for the fast flux and thermal flux with no thermal poison present are shown in Figure 6.1. The ratio of the volume-average fast flux to the volume-average thermal flux in each of the seven regions taken from the FOG output is shown in Table 6.3. The eigenvalue corresponding to this is 1.20.

The flux profiles with a uniform thermal poison present are shown in Figure 6.2. The corresponding values of the ratio of fast flux to thermal flux are indicated for each region in Table 6.4. The thermal poison required to give an eigenvalue of unity is about 0.012 cm^{-1}. It should be noted that the flux profiles still have the

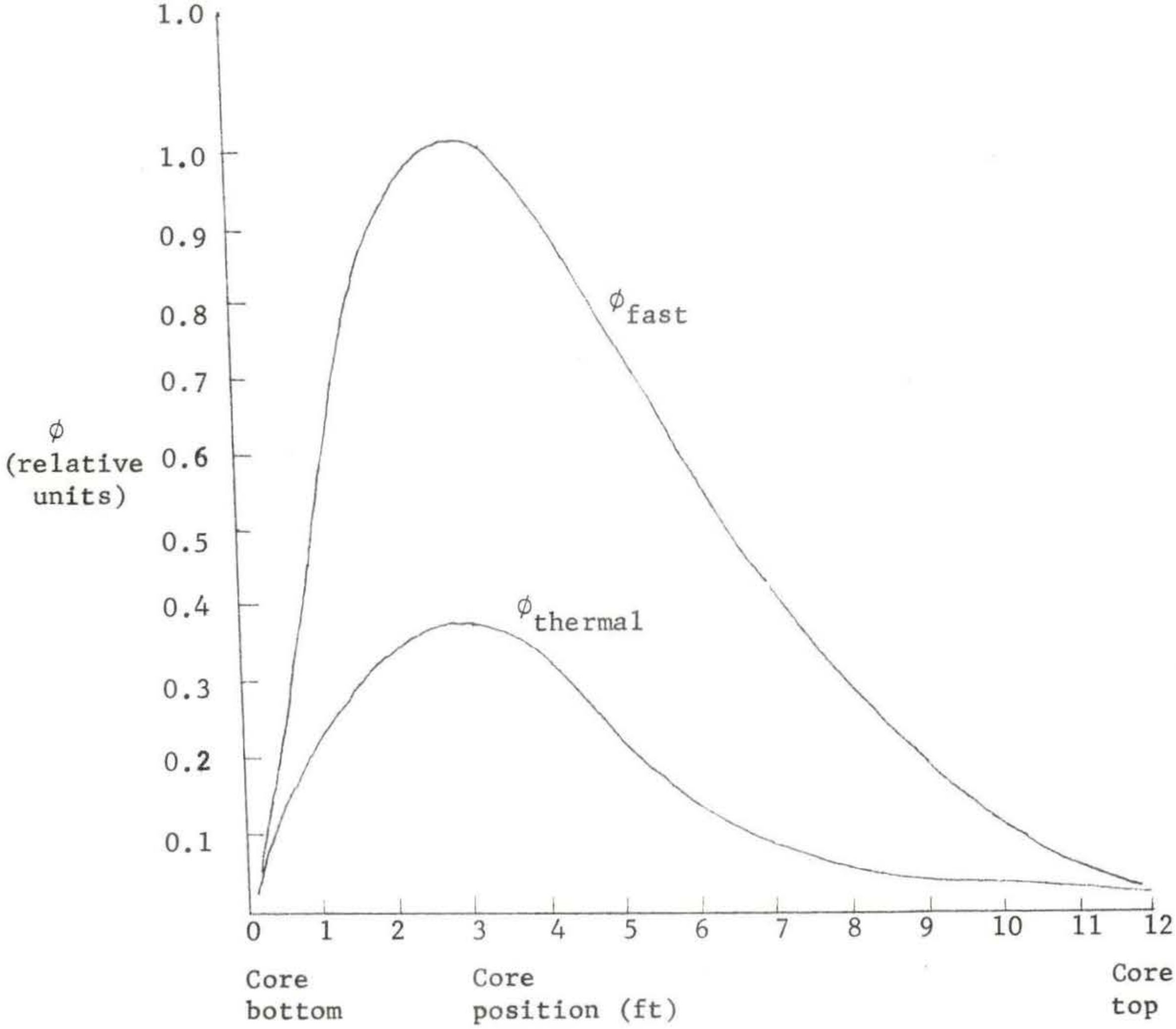

Figure 6.1. Flux profiles with no thermal poison present

same general shape, but that the values of $\phi_{fast}/\phi_{thermal}$ have increased in all regions due to the absorption of thermal neutrons, but not fast neutrons, by the poison.

The flux profiles for a roughly sinusoidal thermal flux are indicated in Figure 6.3. Values of $\phi_{fast}/\phi_{thermal}$ and of Σ_p for each region are shown in Table 6.5.

Table 6.3. $\phi_{fast}/\phi_{thermal}$ with no thermal poison present

Region	$\phi_{fast}/\phi_{thermal}$
1	2.41
2	2.43
3	2.63
4	3.17
5	3.68
6	3.99
7	4.15

To gain a little more understanding of these results, some observations should be made:

1) The axial variation of the values of $\phi_{fast}/\phi_{thermal}$ shown in Table 6.3 indicate the effect of the axial void fraction upon the ratio of fast flux to thermal flux. Physically, this variation is basically due to the loss of moderating ability as a large volume fraction of this coolant becomes vapor bubbles in the upper regions of the BWR fuel bundle.

2) The effect of the addition of a uniform homogeneous thermal poison is to increase the value of $\phi_{fast}/\phi_{thermal}$ uniformly everywhere. The shape of the variation in $\phi_{fast}/\phi_{thermal}$ remains the same. That is, the value of $\phi_{fast}/\phi_{thermal}$ for each region in Table 6.4 is about 1.2 to 1.3 times the value for that same region shown in Table 6.3. The increase in $\phi_{fast}/\phi_{thermal}$ is of course due to the absorption of thermal neutrons, but not fast neutrons, by the thermal poison added.

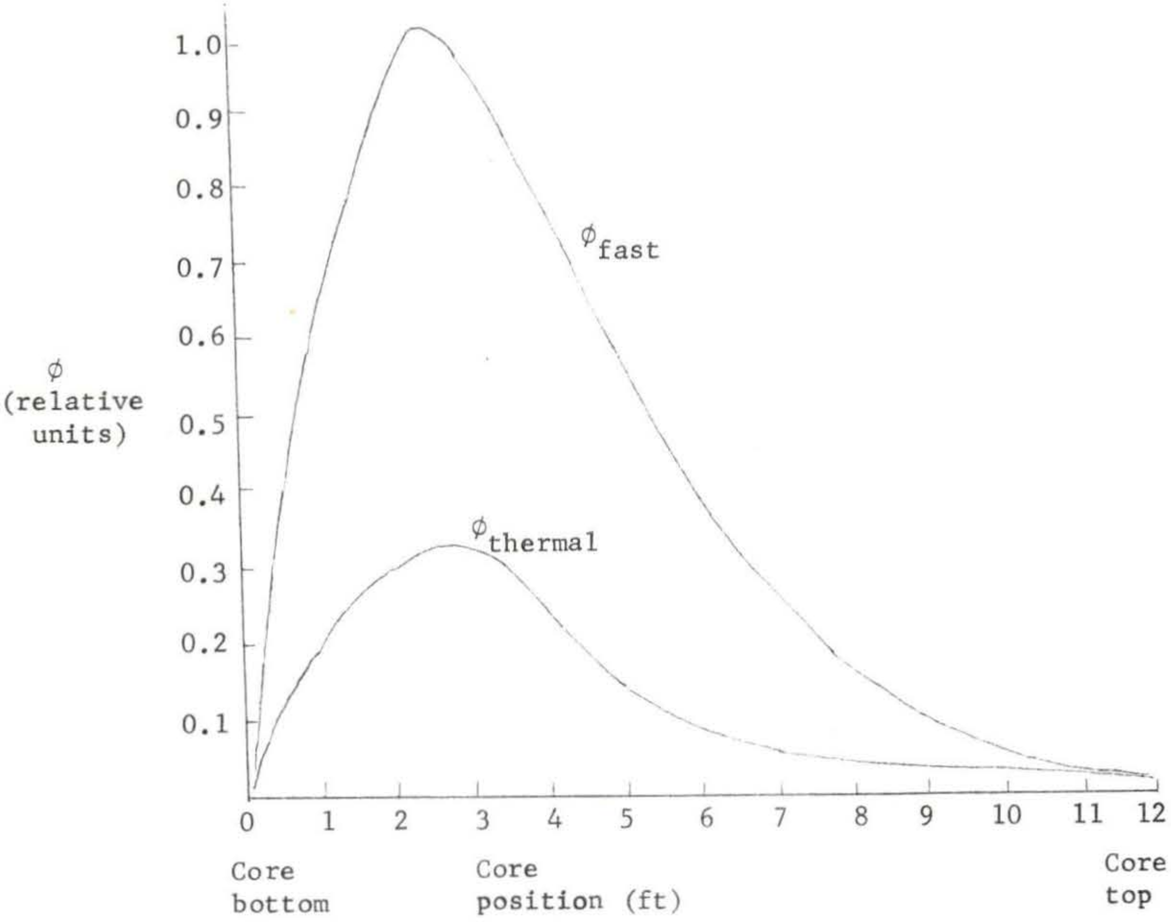

Figure 6.2. Flux profiles with $\Sigma_p = 0.012\ \text{cm}^{-1}$

3) The values of $\phi_{fast}/\phi_{thermal}$ are not particularly sensitive to the shape of the flux, once sufficient thermal poison has been added to make the eigenvalue equal to unity. For example, in Table 6.5, the values when a roughly sinusoidal thermal flux is obtained are only about 5% different from those in Table 6.4. In fact, in making various runs with FOG, little variation in $\phi_{fast}/\phi_{thermal}$ for each region is observed regardless of small changes in flux shape as long as the thermal poison in each region is roughly the same order of magnitude. By the "same order of magnitude," it is meant that Σ_p

Table 6.4. $\phi_{fast}/\phi_{thermal}$ with $\Sigma_p = 0.012\ cm^{-1}$ for all regions

Region	$\phi_{fast}/\phi_{thermal}$
1	2.97
2	3.00
3	3.26
4	3.96
5	4.62
6	5.02
7	5.23

might go from 0.01 cm^{-1} to 0.015 cm^{-1} and result in a different flux shape and still not change $\phi_{fast}/\phi_{thermal}$ very much.

4) It appears from observations made that $\phi_{fast}/\phi_{thermal}$ is primarily a function of the material composition of each region rather than of the flux shape in that region.

Next, consider some practical applications of knowledge of $\phi_{fast}/\phi_{thermal}$ to interpretation of the response of neutron detectors.

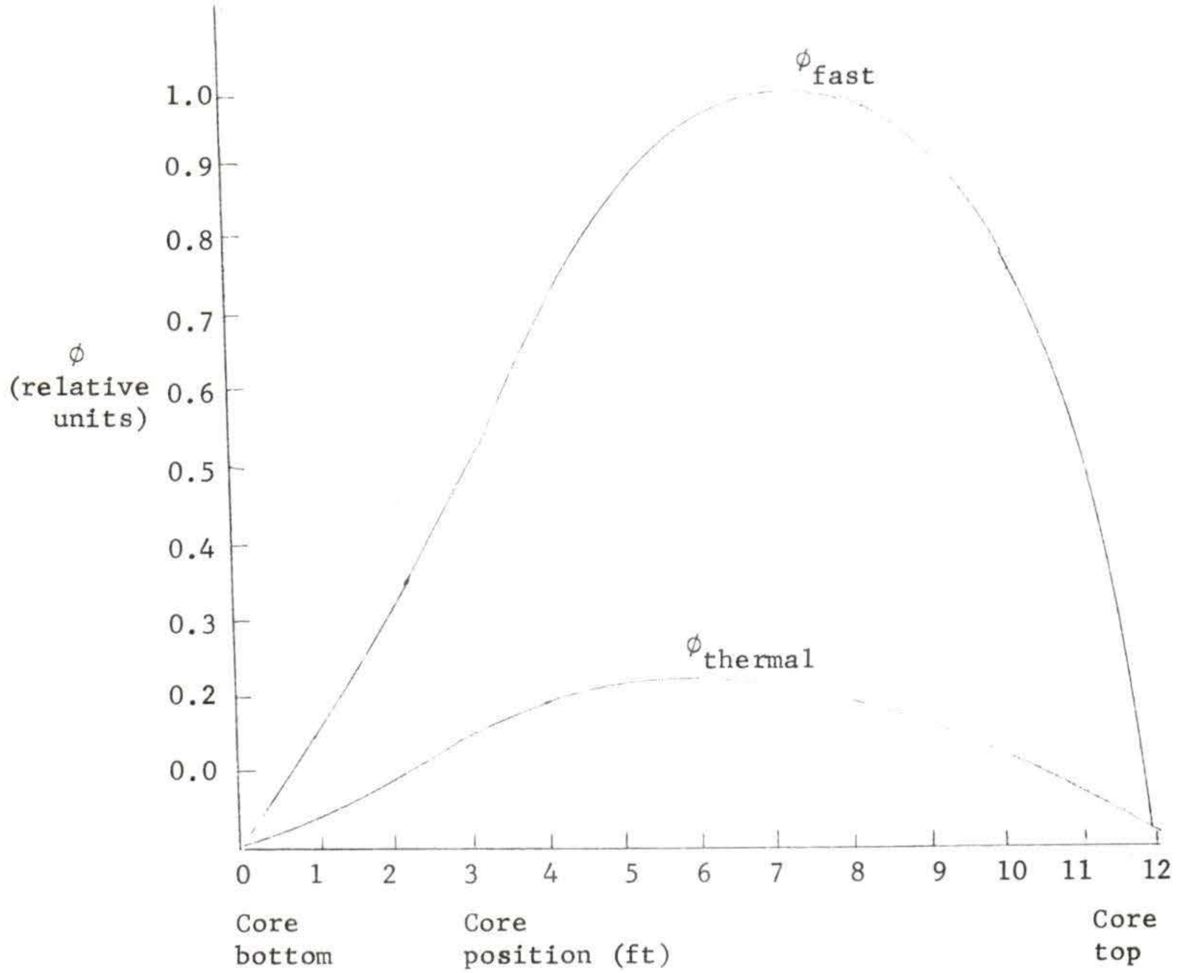

Figure 6.3. Flux profiles for approximately sinusoidal thermal flux

Table 6.5. $\phi_{fast}/\phi_{thermal}$ for approximately sinusoidal thermal flux

Region	Σ_p (cm^{-1})	$\phi_{fast}/\phi_{thermal}$
1	0.015	3.11
2	0.013	3.07
3	0.013	3.33
4	0.012	3.95
5	0.010	4.51
6	0.009	4.80
7	0.008	4.92

VII. APPLICATION OF $\phi_{fast}/\phi_{thermal}$ VALUES TO DETECTOR RESPONSE

A. Introduction

The purpose of this section is to describe two cases of interest where knowledge of the ratio of fast flux to thermal flux may be pertinent to the interpretation of the response of a neutron detector. The first case involves an in-core detector located within a volume of moderator at a certain distance from boundaries where $\phi_{fast}/\phi_{thermal}$ is known. This problem was briefly considered by Hannaman [2]. The second illustration of application of knowledge of $\phi_{fast}/\phi_{thermal}$ involves determining what proportion of the output signal of a self-powered neutron detector located in a reactor core is caused by interactions with the fast flux and what proportion of the signal is caused by interactions with the thermal flux. A description of self-powered neutron detectors and their operation appears in Appendix B. This problem was considered by Jaschik and Seifritz [1].

B. Case 1

The geometry of the detector and its location that Hannaman considered is shown in Figure 7.1. An in-core neutron detector is located within a boiling channel having a known value for the void fraction. The quantity ϕ_1^o/ϕ_2^o is the ratio of the fast flux to the thermal flux at the boundaries ($x = \pm a$) of the volume of moderator containing the detector. Hannaman then considered slab geometry and a point detector in order to simplify his calculations. Then, the two group diffusion equations are:

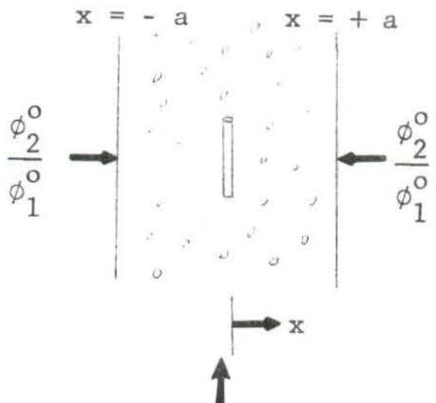

Figure 7.1. Detector geometry used by Hannaman

$$\frac{d^2}{dx^2}\,\phi_1(x) - \frac{\Sigma_1}{D_1}\,\phi_1(x) = 0 \tag{7.1}$$

and

$$\frac{d^2}{dx^2}\,\phi_2(x) - \frac{\Sigma_2}{D_2}\,\phi_2(x) + \frac{\Sigma_1}{D_1}\,\phi_1(x) = 0 \tag{7.2}$$

The solutions to these equations are:

$$\phi_1(x) = A \cosh K_1 x \tag{7.3}$$

where $A = \dfrac{\phi_1^o}{\cosh a}$

$$K_1^2 = \frac{\Sigma_1}{D_1}$$

and

$$\phi_2(x) = \left(\frac{\phi_2^o + \phi_1^o\left(\dfrac{\Sigma_1/D_2}{K_1^2 - K_2^2}\right)}{\cosh K_2 a}\right)\cosh K_2 x - \left(\frac{\phi_1^o\left(\dfrac{\Sigma_1/D_2}{K_1^2 - K_2^2}\right)}{\cosh K_1 a}\right)\cosh K_1 x \tag{7.4}$$

where $K_2^2 = \dfrac{\Sigma_2}{D_2}$

Thus, at the detector position of x = 0:

$$\phi_2(0) = \frac{\phi_2^o + \phi_1^o\left(\frac{\Sigma_1/D_2}{K_1^2 - K_2^2}\right)}{\cosh K_2 a} - \frac{\phi_1^o\left(\frac{\Sigma_1/D_2}{K_1^2 - K_2^2}\right)}{\cosh K_1 a} \tag{7.5}$$

or

$$\phi_2(0) = \phi_2^o\left[\frac{1 + \frac{\phi_1^o}{\phi_2^o}\left(\frac{\Sigma_1/D_2}{K_1^2 - K_2^2}\right)}{\cosh K_2 a} - \frac{\frac{\phi_1^o}{\phi_2^o}\left(\frac{\Sigma_1/D_2}{K_1^2 - K_2^2}\right)}{\cosh K_1 a}\right] \tag{7.6}$$

So, it is seen that in order to determine what thermal flux exists at the position of the point detector, one must have knowledge both of $\phi_{fast}/\phi_{thermal}$ and of Σ_1, Σ_2, D_1, and D_2 for that particular axial position and that particular void fraction. All of these parameters vary significantly with void fraction in a BWR. Thus, a treatment similar to that used in this study would need to be undertaken to obtain information about the parameters.

Recall that in the beginning of Section III it was noted that although the void fraction was treated in a deterministic fashion in this study, it is in truth a variable having random characteristics. Thus, small variations in the void fraction at a particular axial position can occur. One way of obtaining a "feel" for this so-called "void thermalization noise" would be to consider two slightly different void fractions at a particular axial height and see what effect a small change in void fraction had on the thermal flux observed at the detector location.

Next, consider a second case where knowledge of the ratio of fast flux to thermal flux is important.

C. Case 2

Self-powered neutron detectors (see Appendix B) may use a variety of different materials for the emitter material. Cobalt emitters are quite common, and emitters made of erbium, of cadmium, and of hafnium have also been constructed. Such detector materials have significant cross sections for interactions with fast neutrons so that an appreciable fraction of their output signal is produced by the fast flux. Thus, knowledge of $\phi_{fast}/\phi_{thermal}$ is needed if one attempts to determine the fraction of the output due to the fast flux and the fraction due to the thermal flux. The paper by Jaschik and Seifritz [1] gives a detailed model for calculating the response of prompt-responding self-powered neutron detectors that accounts for the following effects:

1) Neutron self-shielding of the emitter

2) Flux depression correction

3) Compton and photoelectron production rate due to self-absorption of the gamma-ray cascade emitted immediately after neutron capture

4) Electron escape probability from the emitter

5) Loss of electron energy within the emitter

6) Range of the electrons in the insulator which contains a space-charge electric field.

To illustrate the difference in emitter materials, consider Table 7.1 which shows the variation in the macroscopic cross section for interactions with neutrons of four different emitter materials. This is data condensed from that of Jaschik and Seifritz [1]. Now, the proportion of the output current caused by either the fast flux or thermal flux

Table 7.1. Neutron interaction cross sections for emitter materials

Emitter material	Σ_{fast} (cm^{-1})	$\Sigma_{thermal}$ (cm^{-1})
Cobalt	1.07	8.89
Cadmium	2.37	435.2
Erbium	8.31	14.0
Hafnium	31.3	13.1

is not simply proportional to these cross sections, but instead is modified by the six effects listed. The ratio of currents that Jaschik and Seifritz [1] finally obtain using a $\phi_{fast}/\phi_{thermal}$ of 3.4 is shown in Table 7.2. Note that in a hafnium detector, a significant fraction of the output current is due to the fast flux. This effect would become even more pronounced in the upper regions of a BWR channel where $\phi_{fast}/\phi_{thermal}$ might be on the order of 5.0. Because of this sensitivity to fast neutrons, hafnium detectors have often been proposed as a void detector in reactor systems.

These two cases that have been presented indicate possible practical applications of knowledge of the magnitude of $\phi_{fast}/\phi_{thermal}$.

Table 7.2. Ratio of output current produced by fast flux and by thermal flux

Emitter material	I_{fast}/I_{total} (%)	$I_{thermal}/I_{total}$ (%)
Cobalt	0.4	99.6
Cadmium	6.0	94.0
Erbium	17.0	83.0
Hafnium	18.3	81.7

VIII. APPROXIMATIONS USED IN STUDY

The purpose of this study is to get a "feel" for the variation of the ratio of fast flux to thermal flux as the void fraction varies up the length of a BWR fuel bundle. In their present state of sophistication, the methods used here are not easily amenable to error analysis to obtain a numerical value of the accuracy involved in their use. Thus, the purpose of this section is to point out some approximations used here and how they differ from the actual situation existing in an operating boiling water reactor producing electrical power. No attempt is made to quantify the accuracy of these approximations.

1) In this study, an unreflected core was considered. In an actual BWR, the core would be reflected by the large volume of water in which the core is submerged. The inclusion of a reflector would be expected to strongly influence the ratio of fast flux to thermal flux at the core bottom and at the core top.

2) In this study, regions were defined having constant material and nuclear properties, such as temperatures, void fraction, diffusion constants and cross sections. In actuality, many of these parameters would have continuous varying axial profiles and, in some cases, radial profiles within a unit cell.

3) LEOPARD treats the reactor as being homogeneous, when the actual reactor is composed of discrete fuel rods, channel walls, and cruciform-shaped control rods.

4) A sinusoidal axial power shape is assumed for the fuel bundle. In reality, power shapes for individual fuel bundles in a BWR may not

be sinusoidal, even though the overall average axial power shape may be sinusoidal.

5) The use of two neutron energy groups is an approximation to the continuous distribution of neutron energies.

6) Poisons are considered to be thermal poisons only, when in reality they would also have some interactions with fast neutrons.

7) The applicability of correlations used in determining the void fraction profile to the flow regime existing within a particular fuel bundle should be verified. The correlations used in this study are generally applicable to slug and/or churn flow in boiling water reactors.

IX. CONCLUSIONS AND SUGGESTIONS FOR FURTHER RESEARCH

A. Conclusions

The following are important conclusions and observations from this study:

1) Consider a fuel bundle with these features:

a) Dimensions like those of the DAEC BWR fuel assemblies

b) An average enrichment of 1.875%

c) Producing power of 3.02×10^5 Btu/hr with a sinusoidal axial distribution

d) With a coolant flow of 2800 lb_m/hr per fuel element

e) With enough thermal poison to produce criticality

f) With no fission products present in the fuel material.

For such a fuel bundle, the ratio of fast flux to thermal flux would appear to vary from about 3 at the core bottom to about 5 at the core top.

2) The shape of the axial variation of $\phi_{fast}/\phi_{thermal}$ is influenced strongly by the axial shape of the void fraction profile.

3) The value of $\phi_{fast}/\phi_{thermal}$ is influenced less strongly by the presence of varying amounts of thermal poison, after sufficient poison is present to override the excess reactivity of the fuel.

4) The major influence upon $\phi_{fast}/\phi_{thermal}$ using volume-average fluxes appears to be the material composition of a particular cross-sectional region of the reactor, rather than the shape of the fluxes in that region.

5) Practical applications of knowledge of $\phi_{fast}/\phi_{thermal}$ have been considered.

B. Suggestions for Further Research

The following are suggestions for further work related to this study that could be pursued:

1) The effects of reflector regions at the core top and the core bottom could be studied. Methods like those of this study could be used.

2) A detailed consideration of the "void thermalization response" of a neutron detector might be pursued. That is, if the geometry of a detector and its location is known, if the average "steady-state" void fraction is known, and if the ratio of fast flux to thermal flux is known, how will the neutron detector respond to a small fluctuation in the void fraction? This might involve using a model like that of Jaschik and Seifritz [1] combined with determination of the effect of a fluctuating void fraction on such a model.

3) One might attempt to study how the ratio of fast flux to thermal flux varies in the close neighborhood of a fuel pin or of a control rod. This would require a treatment that recognizes the discrete nature of a fuel element or control rod rather than homogenizing these components.

4) The effect of axial power shapes other than sinusoidal upon the variation in $\phi_{fast}/\phi_{thermal}$ could be determined. This would seem particularly pertinent because of the widespread use of power flattening and the apparently strong dependence of $\phi_{fast}/\phi_{thermal}$ on void fraction and its dependence on power shape.

5) The effects of burnup of fuel material on the ratio of fast flux to thermal flux could be explored. This would require knowledge of the shape and magnitude of the neutron flux over the time period of interest and correct representation of this shape. This also would require recomputation of cross sections, diffusion parameters, etc. at time steps of interest spanning the time period.

X. LITERATURE CITED

1. Jaschik, W., and W. Seifritz. 1974. Model for calculating prompt-response self-powered neutron detectors. Nucl. Sci. Engr. 53: 61-72.

2. Hannaman, George William, Jr. 1974. Reactor anomaly detection based on noise analysis. Ph.D. Thesis. Iowa State University, Ames, Ia. 169 pp.

3. Dix, Gary E. 1971. Vapor void fractions for forced convection with subcooled boiling at low flow rates. NEDO-10491. (General Electric Atomic Power Equipment Department, San Jose, Cal.) 359 pp.

4. Lahey, R. T., Jr. 1974. Two-phase flow in boiling water nuclear reactors. NEDO-13388. (General Electric Boiling Water Reactor Systems Department, San Jose, Cal.) 108 pp.

5. Stegemann, D., P. Gebureck, A. T. Nikulski, and W. Seifritz. 1973. Operating characteristics of a boiling water reactor deduced from in-core measurements. Pages 15-1 - 15-17 in T. W. Kerlin, ed. Power Plant Dynamics, Control and Testing an Applications Symposium. University of Tennessee, Knoxville, Tennessee.

6. Gebureck, P., W. Hofmann, W. Jaschik, W. Seifritz, and D. Stegemann. 1973. Development and in-core application of self-powered neutron detectors. Paper IAEA-SM-168/G-8. IAEA - Symposium on Nuclear Power Plant Control and Instrumentation. Praque.

7. Holman, J. P. 1968. Heat transfer. McGraw-Hill Book Co., New York, N.Y.

8. Bohl, H., Jr., and A. P. Hemphill. 1961. MUFT-5, a fast neutron spectrum program for the Philco 2000. WAPD-TM-218. (Bettis Atomic Power Laboratory, Pittsburgh, Pa.) 94 pp.

9. Amster, H., and J. B. Kallagan. 1960. KATE-1, a program for calculating Wigner-Wilkins and Maxwellian averaged thermal constants on the Philco-2000. WAPD-TM-232. (Bettis Atomic Power Laboratory, Pittsburgh, Pa.) 57 pp.

10. Crudele, Joseph Samuel. 1973. Study of Ames Laboratory Research Reactor physics characteristics by few group design techniques. Ph.D. Thesis. Iowa State University, Ames, Ia. 119 pp.

11. Strawbridge, L. E. 1963. Calculation of lattice parameters and criticality for uniform water moderated lattices.

WCAP-3269-25. (Westinghouse Atomic Power Division, Pittsburgh, Pa.) 33 pp.

12. Kim, Y. S. 1970. Development of design procedures to determine reactor physics characteristics of high-enriched heavy water moderator reactors. NUS-652. (NUS Corporation, Waltham, Mass.)

13. El-Wakil, M. M. 1971. Nuclear heat transport. Intext Educational Publishers, Scranton, Pa.

14. Barry, R. F. 1963. LEOPARD, a spectrum dependent non-spatial depletion code for the IBM-7094. WCAP-3269-26. (Westinghouse Atomic Power Division, Pittsburgh, Pa.) 65 pp.

15. Munson, Steven T. 1973. The FOG code. M.E. Paper. Iowa State University, Ames, Ia. 63 pp.

16. Flatt, H. P. 1961. The FOG one-dimensional neutron diffusion equation codes. NAA-SR-6104. (Atomics International, Canoga Park, Cal.) 47 pp.

17. Smith, Charles O. 1967. Nuclear reactor materials. Addison-Wesley Publishing Co., Reading, Mass.

18. Babcock and Wilcox Co. 1972. Steam/its generation and use. Babcock and Wilcox Co., New York, N.Y.

19. Welty, James R., Charles E. Wicks, and Robert E. Wilson. Fundamentals of momentum, heat and mass transfer. John Wiley and Sons, Inc., New York, N.Y.

20. Jens, W. H., and P. A. Lottes. 1951. Analysis of heat transfer, burnout, pressure drop, and density data for high pressure water. ANL-4627. (Argonne National Laboratory, Lemont, Ill.) 42 pp.

21. Iowa Electric Light and Power Co. 1972. Final safety analysis report Duane Arnold Energy Center. Author, Cedar Rapids, Iowa.

22. Hsu, Y. Y. 1962. On the size range of active nucleation cavities on a heating surface. J. Heat. Trans. Trans. ASME Ser. C 84(3): 207-216.

23. Gunther, F. C. 1951. Photographic study of surface boiling heat transfer with forced convection. Trans. ASME 73: 115-123.

XI. ACKNOWLEDGMENTS

The author gratefully acknowledges the kind assistance of Dr. Donald M. Roberts in the pursuit of this study and the assistance of the Department of Chemical Engineering and Nuclear Engineering in providing a research assistantship.

XII. APPENDIX A: NUCLEAR SYSTEM DESIGN CHARACTERISTICS FOR DUANE ARNOLD ENERGY CENTER BWR [21]

A. Thermal and Hydraulic Design

Reference design thermal output, Mw(th)	1593
Steam flow rate, lb_m/hr	6.843×10^6
Core coolant flow rate, lb_m/hr	50.5×10^6
Feedwater flow rate, lb_m/hr	6.822×10^6
Feedwater temperature, ^oF	420
System pressure, nominal in steam dome, psia	1020
Average power density, kw/liter	51.0
Maximum thermal output, kw/ft	18.5
Average thermal output, kw/ft	7.067
Maximum heat flux, Btu/hr ft^2	4.276×10^5
Average heat flux, Btu/hr ft^2	1.636×10^5
Maximum UO_2 temperature, ^oF	4430
Average volumetric fuel temperature, ^oF	1210
Average fuel rod surface temperature, ^oF	560
Core maximum exit voids within assemblies, %	76
Core average exit quality, % steam	14.3
Fuel bundle heat transfer area, ft^2	86.67
Core flow area, ft^2	42.2
Specific enthalpy of moderator entering core, Btu/lb_m	526.9
Saturation temperature corresponding to 1020 psia, ^oF	547
Saturated steam density at 1020 psia, lb_m/ft^3	2.37
Saturated liquid density at 1020 psia, lb_m/ft^3	46.5

B. Fuel Design

Fuel rod array	7 × 7
Fuel rod outside diameter, inch	0.563
Fuel rod clad thickness, inch	0.037
Gap — pellet to clad, inch	0.006
Clad material	Zircaloy-2
Fuel pellet material	UO_2
Pellet density, % theoretical	93
Pellet diameter, inch	0.477
Pellet length, inch	0.5
Fuel rod pitch, inch	0.738
Space between fuel rods, inch	0.175
Number of fuel assemblies	368
Number of fuel rods per assembly	49
Overall length of fuel assembly, inches	175.88

C. Fuel Channel

Overall length, inches	166.875
Thickness, inch	0.080
Cross section dimensions (outside), inches	5.438 × 5.438
Material	Zircaloy-4

D. Core Assembly

Equivalent core diameter, inches	129.9
Core height (active fuel), inches	144

XIII. APPENDIX B: SELF-POWERED NEUTRON DETECTORS

The purpose of this section is to give the reader a background on the construction and behavior of self-powered neutron detectors. Self-powered neutron detectors are almost like "little batteries," in that they require no external voltage to power them. Such detectors are particularly useful for in-core detection systems because they are both small and fairly rugged. The usual construction of these detectors is shown in Figure B.1. The three main parts of such a detector are the emitter, the insulator, and the collector. The emitter is generally a metallic material like cobalt or vanadium which gives rise to a signal current due to some sort of interaction between neutrons and the emitter material. The insulator is a ceramic material, with Al_2O_3 powder being used quite often. Finally, the collector is again a metallic material. These components are arranged in a coaxial geometry with overall dimensions of the detector being 10-20 cm in length and 0.15-0.4 cm in diameter. Variations in these dimensions have been studied in research and development work carried out at the Institute für Kerntechnik, Technische Universität, Federal Republic of Germany [6], as well as by others.

Two types of self-powered neutron detectors may be distinguished, based upon the type of interaction between neutrons and the emitter material. The first of these is the so-called prompt-responding self-powered neutron detector. In these SPN detectors, electrons are produced by Compton effect, photo effect, pair production, and conversion electrons. A typical emitter material for this type of SPN detector

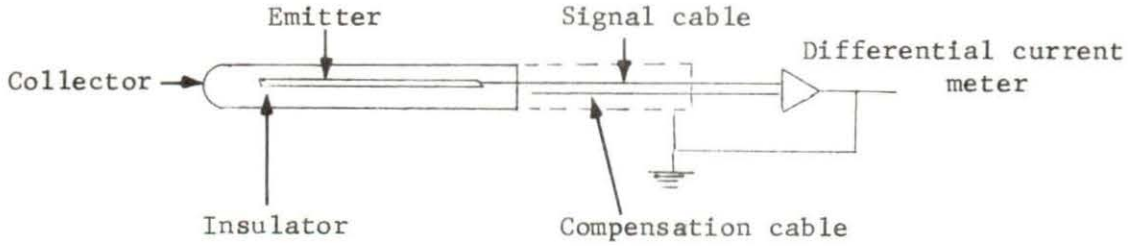

Figure B.1. Self-powered neutron detector schematic

is cobalt. Other suitable materials include erbium and hafnium. The decay scheme for cobalt is shown in Figure B.2. The primary contribution to the signal current in this type of detector is from Compton electrons produced in the interaction of the cascade of prompt capture gamma rays from the decay of $^{60}_{27}Co^*$ to $^{60}_{27}Co$ with surrounding material. Note that it is not the decay of $^{60}_{27}Co$ which constitutes the bulk of the signal, but that rather the electrons from B^- decay constitute a background noise. Thus, this type of detector is basically prompt-responding with the half-life of $^{60}_{27}Co$ having no particular significance.

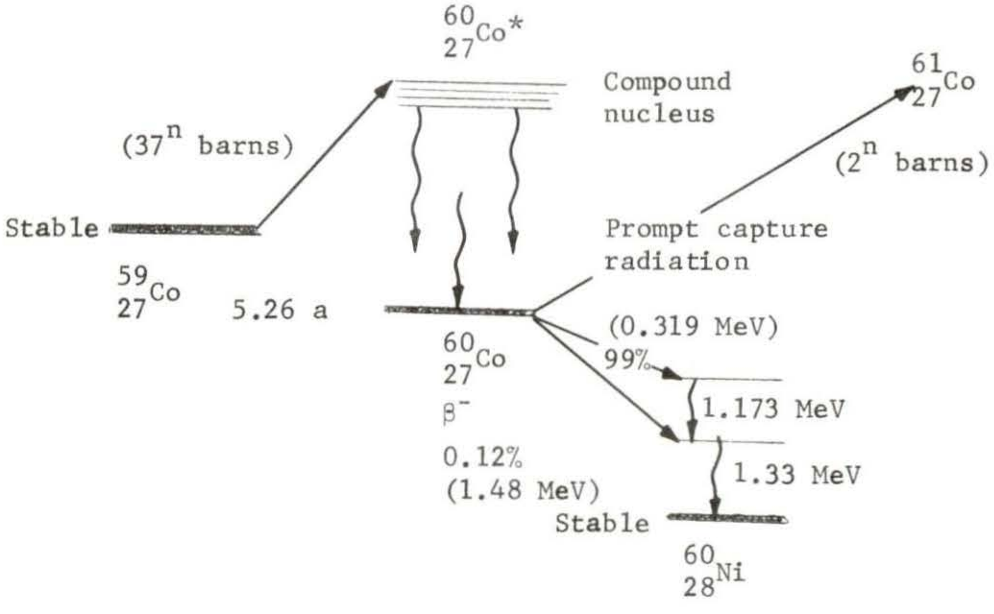

Figure B.2. Cobalt decay scheme

In the second type of SPN detector, the electrons from B^- decay do constitute the bulk of the signal, and thus the half-life of the radionuclide becomes important in determining the time response of the detector. Examples of this type of emitter material include rhodium (Rh^{104}) with a 42-second half-life and vanadium (V^{52}) with a 3.76-minute half-life. If these types of detectors are used to follow changes in neutron level in an operating nuclear reactor, then a time-correction system of some sort must be used or otherwise there will be a smoothing out of sharp changes in the neutron level by the detector response. This smoothing is not desirable if these SPN detectors are to be utilized for neutron noise measurements.

One other point needs to be mentioned with regard to SPN detectors. The sensitivity of the self-powered neutron detector to various portions of the neutron spectrum is dependent on the emitter material used. For example, detectors with a hafnium emitter are more sensitive to fast neutrons than are those with a cobalt emitter. For a hafnium emitter, thermal and fast neutrons make contributions of comparable magnitude to the emitter signal, while for a cobalt emitter, thermal neutrons are the predominant source giving rise to the signal emitted. Because of their particular sensitivity to the fast neutron spectrum, hafnium emitter SPN detectors have been proposed as a method of measuring the void fraction in a boiling water reactor, since the ratio of fast flux to thermal flux is sensitive to the void fraction of the moderator.

Finally, a note on terminology is needed. Detectors having the common principle of detection of electrons leaving an emitter and falling on a collector and entailing the escape of Compton or conversion electrons often are called other names, including "collectrons," "beta-emission detectors," "self-powered neutron detectors," and "electron-emission detectors." The reader should be aware of these terms and recognize the differences where they exist.

XIV. APPENDIX C: BOILING HEAT TRANSFER

The purpose of this section is to give the reader who is somewhat unfamiliar with boiling heat transfer an intuitive feeling for the physical phenomena occurring in the process of boiling and their effects upon the efficiency of heat transfer within a BWR.

The boiling phenomenon can be classified in a variety of ways. Perhaps the first necessary distinction is between "nonflow boiling" and "flow boiling. As the terms suggest, the distinction lies in the existence of, or lack of, net bulk motion of the boiling liquid. Nonflow boiling occurs when a pan of water set upon a stove boils. There is no net bulk motion of the fluid past the heating surface, which in this case would be the bottom and, to some extent, the sides of the pan. In a boiling water nuclear reactor, flow boiling exists because the water is moving past the heating surfaces, the cladding surfaces of the fuel rods. The driving force for flow boiling in a BWR is either due to density differences in a natural circulation BWR or to the pumping force provided by the recirculation pumps and the jet pumps in a forced circulation BWR. The degree to which nonflow boiling is understood is somewhat greater than for flow boiling, primarily because it involves fewer parameters that can vary.

The boiling phenomenon may also be classified as either "pool boiling" or "volume boiling." In pool boiling, heat is added to the liquid by a submerged or adjacent heating surface, such as the bottom of the pan in the above example. In volume boiling, the heat required to vaporize the liquid is generated within the bulk of the liquid by a chemical or nuclear reaction. This type of boiling might occur in a fluid-fuel reactor, such as a water-boiler nuclear reactor.

An important classification of boiling is as "nucleate boiling" or as "film boiling." In nucleate boiling, vapor bubbles originate and grow at small cavities and scratches in the heating surface called nucleation cavities. Heat transfer during this type of boiling is quite good since as each bubble grows and either is released or collapses, cooler liquid rushes in to replace the space occupied by the bubble on the heating surface. The resulting turbulence enhances heat transfer significantly. In film boiling, the vapor forms an insulating film over the heating surface. Because the film transfers heat poorly, the heat transfer from the heating surface is severely diminished.

Nucleate boiling and film boiling are not really separate and unrelated types of phenomena, but rather points along a continuum. They are two of five so-called "boiling regimes." These regimes give rise to the familiar boiling regime curve for nonflow pool boiling shown in Figure C.1. Physically, the boiling regimes may be visualized in the following manner: As boiling begins, the first few nucleation cavities on the heating surface become active and bubbles of vapor begin to form. Depending upon the bulk temperature of nearby liquid, the bubbles will either detach and move away from the heat surface or collapse. Hsu [22] has produced a model which predicts the effective size range of cavities, scratches, pocks, etc. in the heating surface which will serve as active nucleation sites. Inputs to his model include the degree of subcooling, system pressure, physical properties of the liquid and of the heating surface, and the thickness of a superheated thermal layer adjacent to the heating surface.

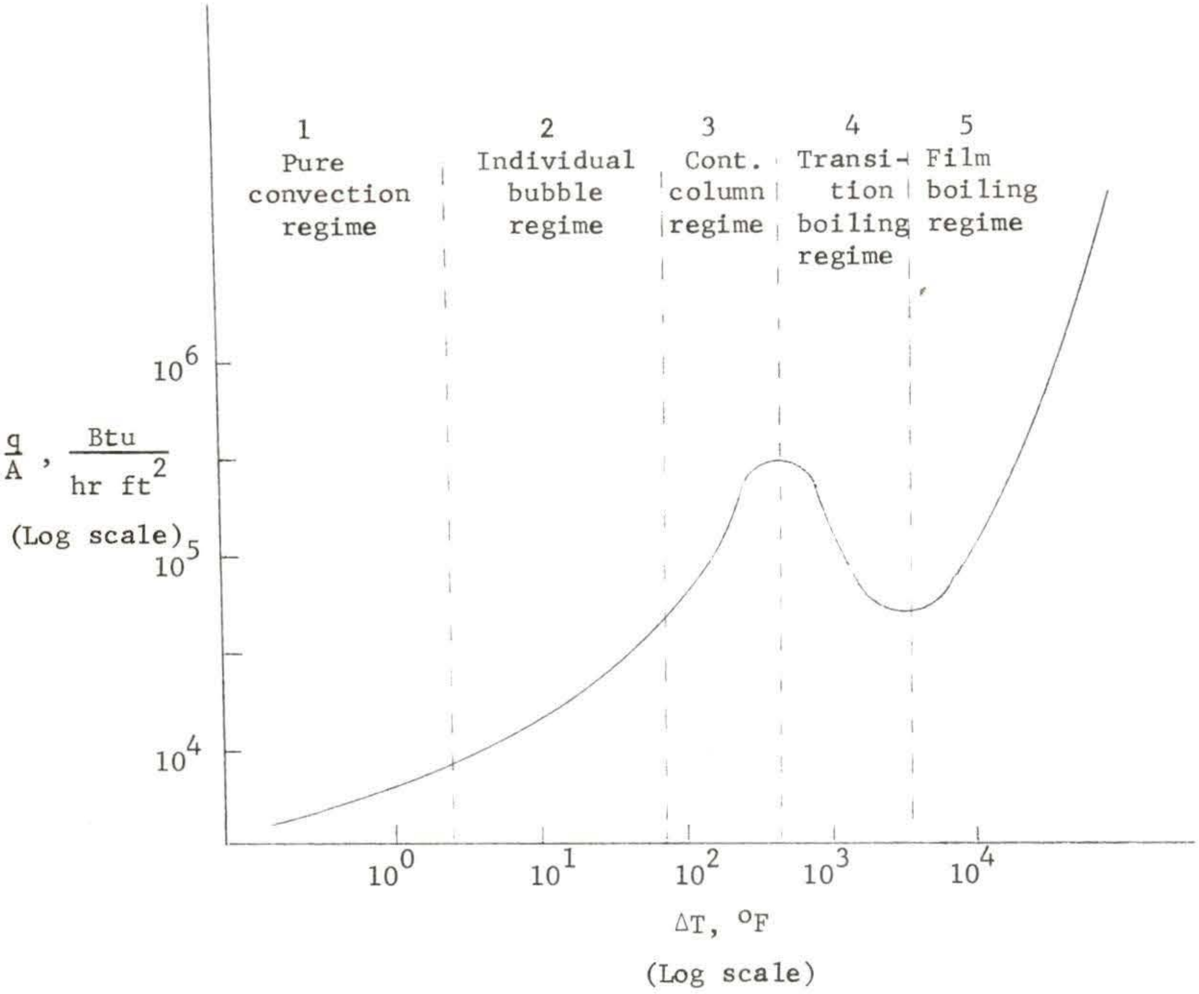

Figure C.1. Typical boiling curve for nonflow, pool boiling at atmospheric pressure

As the temperature of the heating surface continues to increase, more and more cavities on the surface come into play as active nucleation centers. Not only does the number of nucleation centers increase, but the rate of growth and frequency of formation of bubbles also increases. The increased bubble activity and turbulence greatly facilitates heat transfer, as is reflected in the sudden swing upward of the boiling regime curve in Figure C.1. With the increased number and emission rate for the vapor bubbles, some of the bubbles collide and coalesce with their predecessors from a particular nucleation site to form continuous, moving columns of vapor above each active nucleation center.

If the heating surface temperature continues to be raised, the number of active nucleation centers continues to increase until nearly the entire surface is covered by rapidly rising columns of vapor. This marks the transition from nucleate boiling to film boiling. Becoming so crowded with vapor that cooler liquid no longer can move easily to the surface to be heated, the heating surface encounters greater resistance to the transfer of its heat to surrounding liquid. At this point one of several possible events may occur. These are:

1) If the heating surface temperature is the independent variable, or the parameter over which the experimenter can exercise control, the transition from nucleate boiling to stable film boiling will be accomplished and the heat flux through the surface will decrease significantly.

2) If the heat flux is the independent variable, or the controlled variable, the transition to stable film boiling will be marked by a significant rise in the heating surface temperature, provided that temperature remains below the melting point of the material, caused by the insulating effect of the vapor film.

3) If the heat flux is the independent variable and is increased past the value corresponding to the peak of the curve in Figure C.1, the fact that heat is being received faster than it can be dissipated by the heating surface by the film boiling mechanism will cause the surface temperature to rise beyond the melting point of the material

and cause the heating surface to melt. This is called "burnout" and obviously a situation to be avoided in a nuclear reactor.

The above description of boiling applies strictly only to nonflow, pool saturated boiling. Saturated boiling means the surrounding liquid is at saturation temperature. Boiling can also occur for subcooled surrounding liquid if the heating surface temperature is high enough to create a superheated boundary layer in which bubbles can form. The mechanism is quite similar, except that the bubbles increase in number while their size and average lifetime decrease for a decreasing bulk temperature at some constant given heat flux [23].

One other point requires mention with regard to Figure C.1. That curve indicates the average behavior for a particular segment of heating surface under certain conditions of heat flux, subcooling, pressure, etc. Superimposed upon this average behavior may be fluctuations in the bubble generation rate or void content, or in another interpretation, fluctuations in the heat transfer coefficient, h. Thus, when viewing Figure C.1., it should be recognized that actual physical conditions are not represented by just a single point on the curve, but rather by a point plus a small variation in either direction along the curve.

Next, examine more closely bubble formation, growth, and detachment from a heating surface. As already indicated, bubbles are believed to be formed in small pits and cavities called nucleation centers. The greater the number of properly-sized nucleation cavities on a surface, the more enhanced is boiling heat transfer from surface to liquid. Bubble formation is also enhanced by two other "nucleation aids:" (1) The presence of gas or vapor in the surrounding liquid, and (2) the wetting characteristics of the surface. Cavities and scratches are centers for bubble formation because they are usually sharp enough that surface tension forces prevent the entire interior of the cavity from being wetted by the liquid, so that nucleation cavities usually have some gas or vapor entrapped at their bottoms. Such pits and scratches often are also the hottest points in a small neighborhood on the heating surface due to local temperature variations and so may be the first points on the surface able to supply the necessary superheat for bubble formation.

Wetting characteristics of a liquid give information about the amount of contact between a bubble and the heating surface, generally measured by the contact angle, B, defined in Figure C.2. Figure C.3 shows terms used in discussing wettability.

The maximum bubble growth rate and the least degree of superheat required for bubble formation occur for a totally unwetted surface. This is not best, however, for good heat transfer because the bubbles quickly grow and coalesce to form a continuous film barrier without detaching themselves. A more desirable surface is one with many small unwetted areas separated by large patches of partially wetted surfaces. Bubbles would grow rapidly on unwetted surfaces until overlapping to wetted spots where they would then detach. Unwetted spots might be caused by impurities on the surface or by gas adsorption at a material crystal lattice imperfection on the surface. From this discussion, one notes that surface wettability most directly affects bubble detachment from the surface. In nonflow pool boiling, bubble detachment

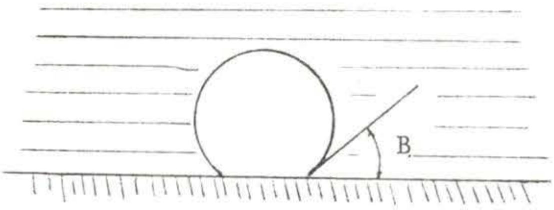

Figure C.2. Bubble contact angle, B

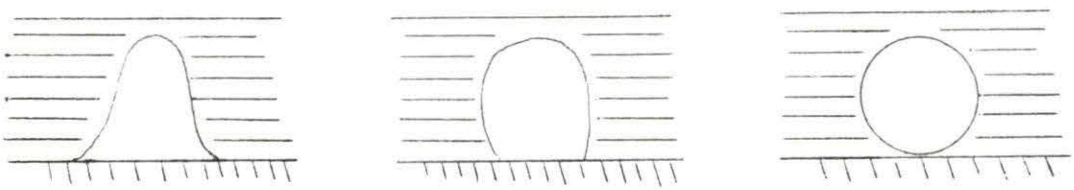

(a) Unwetted, $B > 90^\circ$

(b) Partially wetted, $B < 90^\circ$

(c) Totally wetted, $B \ll 90^\circ$

Figure C.3. Effect of wetting characteristics on bubble contact angle

occurs when it grows large enough for its buoyancy force to overcome the capillary force holding it to the surface. The larger the ratio of a bubble's volume to its surface contact area, the sooner this occurs. Thus, a generally wetted surface has a greater number of smaller bubbles resulting in better heat transfer than for a generally nonwetted surface.

Boiling heat transfer in a BWR is also facilitated by the presence of ionizing radiation and of oxygen and hydrogen produced by radiolysis of the coolant. Ions produced act as nucleation centers and also increase bubble motion and turbulence due to electrical forces between charged bubbles. These nucleation aids are unique to nuclear reactors by their nature.

This completes a brief description of the physical phenomenon of boiling. For a detailed examination of boiling heat transfer with forced convection, the reader may refer to the first portion of Section III of this thesis.